國 立 交 通 大 學

應用數學所

碩 士 論 文

神經網路上的同步方程之

多個穩定狀況的分析

Multistate Stability of Synchronous Equations

in Hindmarsh-Rose Networks

研 究 生： 黃 于 哲

指導教授： 莊 重 教授

中 華 民 國 一 〇 三 年 七 月

神經網路上的同步方程之

多個穩定狀況的分析

Multistate Stability of Synchronous Equations

in Hindmarsh-Rose Networks

研 究 生：黃 于 哲　　Student：Yu-Jhe Huang

指導教授： 莊　 重　　Advisor： Jonq Juang

國 立 交 通 大 學

應 用 數 學 所

碩 士 論 文

A Thesis
Submitted to Department of Applied Mathematics
College of Science
National Chiao Tung University
In Partial Fulfillment of the Requirements
for the Degree of
Master
in
Applied Mathematics

July 2014

Hsinchu, Taiwan, Republic of China

中華民國一〇三年七月

神經網路上的同步方程之
多個穩定狀況的分析

學生：黃 于 哲　　指導教授：莊　重

國立交通大學應用數學學系（研究所）碩士班

摘　　要

在這篇論文中，我們利用幾何奇異擾動理論研究來自 Hindmarsh-Rose 網路之同步化方程的多重穩定狀態。 我們的主要結果如下: 首先，我們給出同步化 Hindmarsh-Rose 方程多重穩定狀態的解釋，例如我們能下結論說在爆裂(bursting)解與具有 canard 現象的週期解能共存。 其次，我們可以充分了解從初始狀態至穩定狀態的過程。 最後，我們可識別出穩定狀態的吸引範圍。 這些都說明了用幾何奇異擾動理論理解實際生物系統的全域動態性質是相當有用的。

關鍵字: 多重穩定狀態、同步化方程、幾何奇異擾動理論。

Multistate Stability of Synchronous Equations in Hindmarsh-Rose Networks

Student: Yu-Jhe Huang Advisors: Jonq Juang

Department of Applied Mathematics
National Chiao Tung University

ABSTRACT

In this thesis, geometric singular perturbation theory is applied to investigate multistate stability of synchronous equations derived from Hindmarsh-Rose Networks. Our main results contain the following. First, explanation of multistability of the synchronous Hindmarsh-Rose equation can be given. For instance, we are able to conclude among other things that a bursting solution and a periodic solution with canard explosion can coexistence. The transition from initial states toward stable states can be fully predicted. Finally, the attraction region with respect to each stable state can be identified. This illustrates the power of using singular perturbation theory to understand the global dynamical properties of realistic biological systems.

Key words: multistate, synchronous equations, geometric singular perturbation theory.

誌 謝

這篇論文的完成，仰賴許多人的幫助與支持，其中以指導老師莊重教授及梁育豪學長對我這個工作的完成幫助最多，莊重老師對我的指導使我對此工作有明確的目標及想法，而梁育豪學長則是幫助我論文中數值相關的部分和一些應注意的細節。 還有我必須感謝同為莊老師學生的黃俊銘學長、林辰燁學長以及謝瑞洸，他們平常或多或少對我的幫助及鼓勵。

在我研究所兩年中，我也必須感謝下列的一些人，同屆的研究生郭柏均、陳學民、江培華、周敬淯以及同間研究室的黃建順、蔡志奇、蔡睿翊，他們對我在研究所的生活有很大的影響。

最後我在此感謝我的父母，他們讓我可以無後顧之憂的作研究。

黃于哲

西元 2014 年 7 月

Table of Contents

1 Introduction

The fundamental building block of every nervous system is the neuron. The behavior of even a single cell can be quite complicated [1], [2] and [3]. For instance, an individual single cell may fire repetitive action potentials or bursts of action potentials that are followed by a silent phase of near quiescent behavior [4]. In the last decades, many biological neuron models have been proposed for an accurate description and prediction of biological phenomena. The pioneering work in such direction is due to Hodgkin and Huxley. To simplify such a model, simpler approximations, namely, the second order systems such as the FitzHugh-Nagumo (FN) and Morris-Lecar neuron models have been proposed. However, the second order models are not able to reproduce some interesting phenomena such as terminating themselves by triggering a set of stable firings. Hence, the Hindmarsh-Rose (HR) model was added a third dynamical component, whose role is to tune the above subsystem over the mono- and bistability regions in order to activate or terminate the neuronal response. The third order system of HR has turned out to be accurate in capturing both qualitative and quantitative aspects of experimental data [5]–[8]. Furthermore, major neuronal behaviors such as spiking, bursting, and chaotic regime have been produced by such HR model [1], [8] and [9].

Example of population rhythms include synchronous behavior, in which easy all in the network fires at the same time, and clustering [10], [11], [12], [13] and [14], in which the entire population of cells breaks up into subpopulations or blocks; every cell within a single block fires synchronously and different blocks are desynchronyed from each other. Neural synchronization has been suggested as particularly relevant for neuronal signal transmission and coding in the brain. Brain [15]–[22] oscillations that are ubiquitous phenomena in all brain areas eventually get into synchrony and consequently allow the brain to process various tasks from cognitive to motor tasks. Indeed, it is hypothesized that synchronous brain activity is the most likely mechanism for many cognitive functions such as attention, feature binding, learning, development, and memory function.

In [23], a new phenomena of the multistate and multistage synchronization of HR neurons with excitatory chemical and electrical synapses over the complex network are analytical studied. In this thesis, we are to use geometric singular perturbation theory to understand such phenomena of multistate synchronization. Specifically, we shall consider the HR networks restricted on its synchronous manifold. The resulting equation is to be termed synchronous equation with respect to HR networks. Our main results contain the following. First, explanation of multistability of the synchronous Hindmarsh-Rose equation can be given. For instance, we are able to conclude among other things that a bursting solution and a periodic solution with canard explosion can coexistence. The transition from initial states toward stable states can be fully predicted. Finally, the attraction region with respect to each sta-

ble state can be identified. This illustrates the power of using singular perturbation theory to understand the global dynamical properties of realistic biological systems.

The thesis is organized as follows. In Section 2, we state some basic facts concerning geometric singular perturbation theory and Hopf bifurcation. The synchronous equation of HR networks and some known properties, observed by computer simulations done in [23], are stated in Section 3. The main results of the thesis is contained in Section 4.

2 Preliminaries

For ease of reference, we introduce the well-known geometric singular perturbation theory. For more details we refer to [24] and [25].

2.1 Geometric Singular Perturbation Theory

2.1.1 Basic Setting

The equations under consideration are of the form

$$\begin{cases} \mathbf{x}' = f(\mathbf{x}, \mathbf{y}, \varepsilon), \\ \mathbf{y}' = \varepsilon g(\mathbf{x}, \mathbf{y}, \varepsilon), \end{cases} \tag{1}$$

where $' = \dfrac{d}{dt}$, $\mathbf{x} \in \mathbb{R}^n$, $\mathbf{y} \in \mathbb{R}^m$ and $\varepsilon \in \mathbb{R}$ is a small parameter $(0 < \varepsilon \ll 1)$ which gives the equations a singular character.
The following statement is one of the basic assumptions:

Hypothesis 1. The functions f and g are both assumed to be C^r on a set $U \times I$, where $U \subset \mathbb{R}^{n+m}$ is open and I is an open interval, containing 0 and $r \geq 1$.

From (1), let $s = \varepsilon t$, then equation (1) is transformed to the following form

$$\begin{cases} \varepsilon \dot{\mathbf{x}} = f(\mathbf{x}, \mathbf{y}, \varepsilon), \\ \dot{\mathbf{y}} = g(\mathbf{x}, \mathbf{y}, \varepsilon), \end{cases} \tag{2}$$

where $\dot{} = \dfrac{d}{ds}$. The time scale given by s is said to be slow whereas that for t is fast. In fact, as long as $\varepsilon \neq 0$ the two systems are equivalent. Thus we call (1) the **fast system** and (2) the **slow system**.
Letting $\varepsilon \longrightarrow 0$, that the limiting systems of (1) and (2) are, respectively,

$$\begin{cases} \mathbf{x}' = f(\mathbf{x}, \mathbf{y}, 0), \\ \mathbf{y}' = \mathbf{0}, \end{cases} \tag{3}$$

and

$$\begin{cases} f(\mathbf{x}, \mathbf{y}, 0) = \mathbf{0}, \\ \dot{\mathbf{y}} = g(\mathbf{x}, \mathbf{y}, 0). \end{cases} \tag{4}$$

Let $N = \{ (\mathbf{x}, \mathbf{y}) \in U \mid f(\mathbf{x}, \mathbf{y}, 0) = \mathbf{0} \}$. In view of system (3), each point of N is a fixed point and the system (3) has nontrivial dynamical behaviors on $U \backslash N$. On the other hand, system (4), defined only on N, usually has nontrivial dynamical behaviors on N. We next define the concept of a set being normally hyperbolic

Definition 1. Let $M_0 \subset N$. The set M_0 is said to be **normally hyperbolic** if $D_{\mathbf{x}} f(\tilde{\mathbf{x}}, \tilde{\mathbf{y}}, 0)$ has exactly n eigenvalues λ with $\mathrm{Re}(\lambda) \neq 0$ for any $(\tilde{\mathbf{x}}, \tilde{\mathbf{y}}) \in M_0$.

Hypothesis 2. Let $M_0 \subset N$. The set M_0 is assumed to be a compact manifold and is normally hyperbolic.

The set M_0 will be called the **critical manifold**.

Since from Hypotheses 2, we have that $D_{\mathbf{x}} f(\tilde{\mathbf{x}}, \tilde{\mathbf{y}}, 0)$ is invertible for any $(\tilde{\mathbf{x}}, \tilde{\mathbf{y}}) \in M_0$. By the Implicit Function Theorem, $\mathbf{x}$ can locally be solved for $\mathbf{y}$, that is, $\mathbf{x} = h^0(\mathbf{y})$ for some smooth function h^0. Since the set which is a graph of some smooth function is easier to manipulate, we want to decompose M_0 into a finite number of its subset that is a graph of some smooth function and satisfies Hypotheses 2. (i.e. $M_0 = M_0^{(1)} \cup M_0^{(2)} \cup \cdots \cup M_0^{(k)}$ where $M_0^{(i)}$ is a graph of some smooth function and satisfies Hypotheses 2 for i=1,2,. . . , k.
In order to simplify discussion, we consider that M_0 is a graph of function satisfying the following two hypotheses.

Hypothesis 3. M_0 is normally hyperbolic and there are a compact subset K of $\mathbb{R}^m$ and a function h^0 defined on K such that $M_0 = \{ (\mathbf{x}, \mathbf{y}) \in U \mid \mathbf{x} = h^0(\mathbf{y}) \}$.

Hypothesis 4. h^0 is a smooth function on K and K is simply connected domain whose boundary is an $(m-1)$-dimensional C^∞ submanifold.

In addition, we also assume that the following hypothesis holds.

Hypothesis 5. $D_{\mathbf{x}} f(\tilde{\mathbf{x}}, \tilde{\mathbf{y}}, 0)$ has ℓ eigenvalues λ with $\mathrm{Re}(\lambda) < 0$ and $k (= n - \ell)$ eigenvalues λ with $\mathrm{Re}(\lambda) > 0$ for any $(\tilde{\mathbf{x}}, \tilde{\mathbf{y}}) \in M_0$.

2.1.2 Fenichel's Theorems

We give some definitions and some notations in order to state Fenichel's Theorems.

Notation. The notation $\mathbf{x} \cdot t$ is used to denote the application of a flow after time t to the initial condition $\mathbf{x}$. Similarly, $V \cdot t$ denote the application of a flow after time t to a set V, and $\mathbf{x} \cdot [t_1, t_2]$ is the resulting trajectory if the flow is applied over the interval $[t_1, t_2]$.

Definition 2. A set M is **locally invariant** under the flow from (1) if there exists a neighbourhood V of M so that for all $\mathbf{x} \in M$, $\mathbf{x} \cdot [0,t] \subset V$ implies that $\mathbf{x} \cdot [0,t] \subset M$, similarly with $[0,t]$ replaced by $[t,0]$ when $t < 0$.

Theorem 1. (Fenichel's First Theorem, see e.g., [24])
Under the Hypotheses 1 and 2. Then for $\varepsilon > 0$ and sufficiently small, there exists a manifold M_ε that lies within $O(\varepsilon)$ of M_0 and is diffeomorphic to M_0. Moreover it is locally invariant under the flow of system (1), and C^r, including in ε, for any $r < +\infty$.

The manifold M_ε will be called the **slow manifold**.

Theorem 2. (Fenichel's First Theorem for graph version, [24])
Under the Hypotheses 1, 3 and 4. Then for $\varepsilon > 0$ and sufficiently small, there exists a function h^ε, defined on K, so that $M_\varepsilon = \{(\mathbf{x}, \mathbf{y}) \,|\, \mathbf{x} = h^\varepsilon(\mathbf{y}), \mathbf{y} \in K\}$ is locally invariant under the flow of system (1). Moreover h^ε is C^r, for any $r < +\infty$, jointly in $\mathbf{y}$ and ε.

Remark. The diffeomorphism between M_ε and M_0 follows easily in this formulation through the diffeomorphism of the graph to K.

Flow on M_ε:

$$\mathbf{y}' = \varepsilon g(h^\varepsilon(\mathbf{y}), \mathbf{y}, \varepsilon). \tag{5}$$

In the alternative slow scaling we recast (5) as

$$\dot{\mathbf{y}} = g(h^\varepsilon(\mathbf{y}), \mathbf{y}, \varepsilon). \tag{6}$$

which has distinct advantage that a limit exists as $\varepsilon \to 0$, given by $g(h^0(\mathbf{y}), \mathbf{y}, 0)$ which naturally describes a flow on the critical manifold M_0, and is exactly the second equation in (2). Using this theorem and this resulting equation (6), the problem of studying (1), at least on M_ε is reduced to a regular perturbation problem.

Example. Consider the system

$$\begin{cases} \dot{u}_1 = u_2 \\ \dot{u}_2 = u_3 \\ \varepsilon \dot{u}_3 = u_4 \\ \varepsilon \dot{u}_4 = u_5 \\ \varepsilon \dot{u}_5 = u_6 \\ \varepsilon \dot{u}_6 = -A u_5 - u_3 - c u_2 - f(u_1), \end{cases}$$

where $A > 0$, $f(\phi) = \phi(\phi - a)(1 - \phi)$, $a < \frac{1}{2}$, c: constant.

Let $\mathbf{x} = \begin{bmatrix} u_3 \\ u_4 \\ u_5 \\ u_6 \end{bmatrix}$, $\mathbf{y} = \begin{bmatrix} u_1 \\ u_2 \end{bmatrix}$ then $\mathbf{x}$ is the fast variable and $\mathbf{y}$ is the slow variable.

The critical manifold M_0 can be taken as any compact subset of $\{u_4 = u_5 = u_6 = 0,\ u_3 = -cu_2 - f(u_1)\}$ and will shall be large enough to contain any of the dynamics of interest.
The eigenvalues of linearization at any point of M_0, other than the double eigenvalue at 0 are seen to be solutions of quartic equation $\mu^4 + A\mu^2 + 1 = 0$ which are not pure imaginary if $0 < A < 2$.
The equation for the slow flow on the critical manifold M_0 are given by $\begin{cases} \dot{u}_1 = u_2, \\ \dot{u}_2 = -cu_2 - f(u_1). \end{cases}$
The slow manifold M_ε, which exists by virtue of theorem 1,is given by the equations

$$(u_3, u_4, u_5, u_6) = h^\varepsilon(u_1, u_2) = (-cu_2 - f(u_1), 0, 0, 0) + O(\varepsilon)$$

and the equations on M_ε are $\begin{cases} \dot{u}_1 = u_2, \\ \dot{u}_2 = -cu_2 - f(u_1) + O(\varepsilon). \end{cases}$

We know nothing of the flow off the slow manifold and this must now be addressed. The slow manifold possesses accompanying stable and unstable manifolds that are perturbations of the corresponding manifolds when $\varepsilon = 0$.

Theorem 3. (Fenichel's Second Theorem, see e.g., [25])
Under the Hypotheses 1 and 2. Then for $\varepsilon > 0$ and sufficiently small, there exists manifolds $W^s(M_\varepsilon)$ and $W^u(M_\varepsilon)$ that are $O(\varepsilon)$ close and are diffeomorphic to $W^s(M_0)$ and $W^u(M_0)$ respectively, and they are each locally invariant under the flow of system (1), and C^r, including in ε, for any $r < \infty$.

We want to state Fenichel's Second Theorem for graph version but we need a detailed analysis and more notations. So we postpone this after Fenichel's third Theorem. The following is talking about a motivation for Fenichel's third Theorem.
First, we observe that

$$W^s(M_0) = \bigcup_{\mathbf{v}_0 \in M_0} W^s(\mathbf{v}_0),\ W^u(M_0) = \bigcup_{\mathbf{v}_0 \in M_0} W^u(\mathbf{v}_0)$$

In other words, the manifolds $W^s(\mathbf{v}_0)$ and $W^u(\mathbf{v}_0)$ form collections of fibers for $W^s(M_0)$ and $W^u(M_0)$, respectively, with base points $\mathbf{v}_0 \in M_0$.
Second, a natural question to ask now, is whether the individual stable and unstable manifolds $W^s(\mathbf{v}_0)$ and $W^u(\mathbf{v}_0)$ perturb to analogous objects ? —— Fenichel's third Theorem answers this question. In order to avoid difficulties we restrict ourselves to a neighbourhood D of M_ε in which the linear terms of (1) are dominant, and consider only trajectories in $W^u(M_\varepsilon)$ that have not left D in forward time (yet), and trajectories in $W^s(M_\varepsilon)$ that have not left D in backward time. To facilitate this discussion, we need a definition.

Definition 3. The forward evolution of a set $V \subset D$ restricted to D is given by the set

$$V \cdot_D t \equiv \{\, \mathbf{x} \cdot t \,|\, \mathbf{x} \in V \text{ and } \mathbf{x} \cdot [0, t] \subset D \,\}.$$

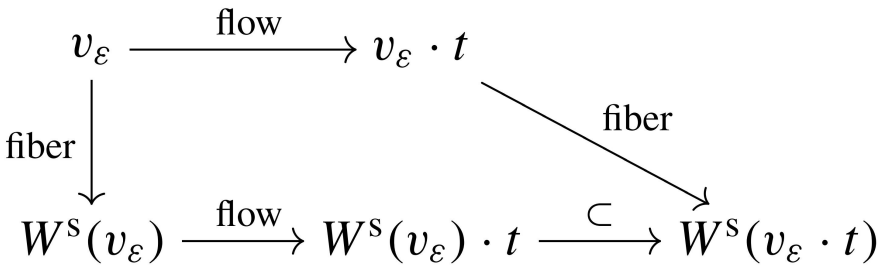

Figure 1: A diagram for Fenichel's Third Theorem.

Now, we sate Fenichel's Third Theorem.

Theorem 4. [Fenichel's Third Theorem][1]
Under the Hypotheses 1, 2 and 5. Then if $\varepsilon > 0$ and sufficiently small then for every $\mathbf{v}_\varepsilon \in M_\varepsilon$ there are an ℓ-dimensional manifold $W^s(\mathbf{v}_\varepsilon) \subset W^s(M_\varepsilon)$ and an k-dimensional manifold $W^u(\mathbf{v}_\varepsilon) \subset W^u(M_\varepsilon)$, that are $O(\varepsilon)$ close and diffeomorphic to $W^s(\mathbf{v}_0)$ and $W^u(\mathbf{v}_0)$ respectively.
Moreover, they are C^r for any r, including in $\mathbf{v}$ and ε.
The families $\{ W^s(\mathbf{v}_\varepsilon) \,|\, \mathbf{v}_\varepsilon \in M_\varepsilon \}$ and $\{ W^u(\mathbf{v}_\varepsilon) \,|\, \mathbf{v}_\varepsilon \in M_\varepsilon \}$ are invariant in the sense that

$$W^s(\mathbf{v}_\varepsilon) \cdot_D t \subset W^s(\mathbf{v}_\varepsilon \cdot t)$$

if $\mathbf{v}_\varepsilon \cdot s \in D$ for all $s \in [0, t]$ $(t > 0)$ and

$$W^u(\mathbf{v}_\varepsilon) \cdot_D t \subset W^u(\mathbf{v}_\varepsilon \cdot t)$$

if $\mathbf{v}_\varepsilon \cdot s \in D$ for all $s \in [t, 0]$ $(t < 0)$.

The idea is, that the order in which the flow after time t is applied to a base point and the fiber of a base point is constructed does not matter, as depicted in this figure (1).
In the unperturbed setting (1) with $\varepsilon = 0$, the decay in forward time of points in $W^s(M_0)$ to M_0 is clearly to the base point $\mathbf{v}_0$ of their fiber, where the decay rate as $t \to \infty$ is exponential, since all associated eigenvalues have nonzero real part.

The fibers give a very useful matching between the points in $W^s(M_\varepsilon)$ and partners they have in M_ε. One can then see that the decay of points in $W^s(M_\varepsilon)$ to M_ε is actually to the base point of the fiber, this gives a decay result with "asymptotic phase"; similarly for points in $W^u(M_\varepsilon)$.

Preparation for statement of Fenichel's Second Theorem for graph version

Suppose that M_0 satisfies the Hypotheses 1, 3 and 4. Without loss of generality, we can assume that $h^0(\mathbf{y}) = \mathbf{0}$ for all $\mathbf{y} \in K$. Indeed, we can replace $\mathbf{x}$ by $\hat{\mathbf{x}} = \mathbf{x} - h^0(\mathbf{y})$

[1] we may refer to [25], P. 376

and recompute the equations. For each $\mathbf{y} \in K$, there are subspaces $S(\mathbf{y})$ and $U(\mathbf{y})$, corresponding, respectively, to stable and unstable eigenvalues. Since the eigenvalues are bounded uniformly away from the imaginary axis over K, the dimensions of $S(\mathbf{y})$ and $U(\mathbf{y})$ are independent of $\mathbf{y}$. Let $\dim S(\mathbf{y}) = \ell$ and $\dim U(\mathbf{y}) = k$. Since K is simply connected by hypothesis 4, we can smoothly choose bases for $S(\mathbf{y})$ and $U(\mathbf{y})$. Changing the coordinates to in terms of these new bases, we can set $\mathbf{x} = (\mathbf{a}, \mathbf{b})$, where $\mathbf{a} \in \mathbb{R}^\ell$ and $\mathbf{b} \in \mathbb{R}^k$, so that our equations have the form

$$\begin{cases} \mathbf{a}' = A(\mathbf{y})\mathbf{a} + F_1(\mathbf{x}, \mathbf{y}, \varepsilon), \\ \mathbf{b}' = B(\mathbf{y})\mathbf{b} + F_2(\mathbf{x}, \mathbf{y}, \varepsilon), \\ \mathbf{y}' = \varepsilon g(\mathbf{x}, \mathbf{y}, \varepsilon), \end{cases} \tag{7}$$

where $\sigma(A(\mathbf{y})) \subset \{\lambda \,|\, \mathrm{Re}(\lambda) < 0\}$ and $\sigma(B(\mathbf{y})) \subset \{\lambda \,|\, \mathrm{Re}(\lambda) > 0\}$. Both F_1 and F_2 consist of any higher order terms in $\mathbf{x}$, $\mathbf{y}$ for each ε; to be precise, we have the estimates $|F_i| \leq \gamma(|\mathbf{x}| + \varepsilon)$, $i = 1, 2$ and γ can be taken to be as small as desired by restricting to a set with $|\mathbf{a}|$ and $|\mathbf{b}|$ small.
With this notation established, we can determine $W^s(M_\varepsilon)$ and $W^u(M_\varepsilon)$ as graphs and give the following restatement of theorem 3.

Theorem 5 (Fenichel's Second Theorem for graph version)**.** [2]
If $\varepsilon > 0$, but sufficiently small, then ,for some $\Delta > 0$,

(a) there is a function $\mathbf{a} = h_s(\mathbf{b}, \mathbf{y}, \varepsilon)$ defined for $\mathbf{y} \in K$ and $|\mathbf{b}| \leq \Delta$, so that the graph $W^s(M_\varepsilon) = \{(\mathbf{a}, \mathbf{b}, \mathbf{y}) \,|\, \mathbf{a} = h_s(\mathbf{b}, \mathbf{y}, \varepsilon)\}$ is locally invariant under (7). Moreover, $h_s(\mathbf{b}, \mathbf{y}, \varepsilon)$ is C^r in $(\mathbf{b}, \mathbf{y}, \varepsilon)$ for any $r < +\infty$.

(b) there is a function $\mathbf{b} = h_u(\mathbf{a}, \mathbf{y}, \varepsilon)$ defined for $\mathbf{y} \in K$ and $|\mathbf{b}| \leq \Delta$, so that the graph $W^u(M_\varepsilon) = \{(\mathbf{a}, \mathbf{b}, \mathbf{y}) \,|\, \mathbf{b} = h_u(\mathbf{a}, \mathbf{y}, \varepsilon)\}$ is locally invariant under (7). Moreover, $h_u(\mathbf{a}, \mathbf{y}, \varepsilon)$ is C^r in $(\mathbf{a}, \mathbf{y}, \varepsilon)$ for any $r < +\infty$.

These theorems also apply when $\varepsilon = 0$ and provide the stable and unstable manifolds of the known critical manifold, the existence of which is also guaranteed by the usual stable and unstable manifold theorems at critical points. These latter two theorems then assert that these manifolds, $W^s(M_\varepsilon)$ and $W^u(M_\varepsilon)$, are perturbed from $W^s(M_0)$ and $W^u(M_0)$ respectively. Theorem 1 can be concluded from Theorem 3 by taking the intersection of $W^s(M_\varepsilon)$ with $W^u(M_\varepsilon)$. Locally, the Implicit Function Theorem gives the intersection as a graph, and these functions can be patched together since K is a compact set. Moreover, we need only give the stable manifold, as that of the unstable manifold follows immediately by a reversal of time.

2.2 Hopf Bifurcation

In this subsection, we review Hopf Bifurcation. For more details we refer to [26].

[2] we may refer to [24], P. 63

2.2.1 Basic assumptions

First, we consider a continuous-time system depending on a parameter.

$$\dot{x} = f(x, \mu),\ x \in \mathbb{R}^n,\ \mu \in \mathbb{R}, \tag{8}$$

where f is smooth with respect to both x and μ. If $x = x_0$ be a hyperbolic equilibrium in the system for $\mu = \mu_0$ then under a small parameter variation the equilibrium moves slightly but remains hyperbolic. In general, there are only two ways in which the hyperbolicity condition can be violated. Either a simple real eigenvalue approaches zero and we have $\lambda_1 = 0$, or a pair of simple complex eigenvalues reaches the imaginary axis and we have $\lambda_{1,2} = \pm i\omega_0$, $\omega_0 > 0$ for some value of the parameter.

Definition 4. We say that a fixed point of the system (8) has the *Hopf* (or *Poincaré–Andronov–Hopf*) *bifurcation* at $\mu = \mu_0$ if a fixed point of the system (8) at $\mu = \mu_0$ has $\lambda_{1,2} = \pm i\omega_0$, $\omega_0 > 0$ and a small perturbation at $\mu = \mu_0$ results in stable or unstable limit cycle from the fixed point.

We suppose that the system (8) satisfy the following assumptions.

Assumption 1. Assume that $(0, 0) \in \mathbb{R}^n \times \mathbb{R}$ is the fixed point of (8), i.e., $f(0, 0) = 0$.

Assumption 2. Assume that $D_x f(0, 0)$ has two purely imaginary eigenvalues with the remaining $n - 2$ eigenvalues having nonzero real parts.

2.2.2 Example

Example. Consider the following planar system depending on one parameter μ:

$$\begin{cases} \dot{x} = -y + \mu x - x(x^2 + y^2), \\ \dot{y} = x + \mu y - y(x^2 + y^2), \end{cases} \tag{9}$$

This system has the equilibrium $(0, 0)$ for all μ with the Jacobian matrix

$$A = \begin{bmatrix} \mu & -1 \\ 1 & \mu \end{bmatrix}$$

having eigenvalues $\lambda_{1,2} = \mu \pm i$. For $\mu = 0$, the linearized equations of system (9) have a center, and as μ varies from negative to positive, the fixed point changes from a stable focus to an unstable focus. Thus the system (9) has a Hopf bifurcation at $\mu = 0$.
In polar coordinates,

$$\begin{cases} \dot{r} = \mu r - r^3, \\ \dot{\theta} = 1. \end{cases}$$

We see that at $\mu = 0$ the system has a stable focus at origin and for $\mu > 0$ the system has a stable limit cycle

$$\gamma_\mu(t) = \sqrt{\mu}\,(\cos t, \sin t).$$

2.2.3 Center manifold reduction

Under assumptions 1 and 2, by the center manifold theorem, we know that the orbit structure near $(x, \mu) = (0, 0)$ is determined by the vector field (8) restricted to the center manifold. This restriction gives us a one-parameter family of vector fields on a two-dimensional center manifold. On the center manifold the vector field (8) has the following form

$$\begin{bmatrix} \dot{x}_1 \\ \dot{x}_2 \end{bmatrix} = \begin{bmatrix} \operatorname{Re}\lambda(\mu) & -\operatorname{Im}\lambda(\mu) \\ \operatorname{Im}\lambda(\mu) & \operatorname{Re}\lambda(\mu) \end{bmatrix} \begin{bmatrix} x_1 \\ x_2 \end{bmatrix} + \begin{bmatrix} g_1(x_1, x_2, \mu) \\ g_2(x_1, x_2, \mu) \end{bmatrix}, \tag{10}$$

$(x_1, x_2, \mu) \in \mathbb{R} \times \mathbb{R} \times \mathbb{R}$ and where g_1 and g_2 are nonlinear in x_1 and x_2 and $\lambda(\mu)$, $\overline{\lambda(\mu)}$ are the eigenvalues of the vector field linearized about the fixed point at the origin. Let $\lambda(\mu) = \alpha(\mu) + i\omega(\mu)$ then, by assumption, we have $\alpha(0) = 0$ and $\omega(0) \neq 0$.

2.2.4 Preparation for statement of the Poincaré–Andronov–Hopf Bifurcation theorem

We transform (10) into normal form. The normal form was found to be

$$\begin{aligned} \dot{x} &= \alpha(\mu)x - \omega(\mu)y + (a(\mu)x - b(\mu)y)(x^2 + y^2) + \mathcal{O}(|x|^5, |y|^5), \\ \dot{y} &= \omega(\mu)x + \alpha(\mu)y + (b(\mu)x + a(\mu)y)(x^2 + y^2) + \mathcal{O}(|x|^5, |y|^5). \end{aligned} \tag{11}$$

In polar coordinates (11) is given by

$$\begin{aligned} \dot{r} &= \alpha(\mu)r + a(\mu)r^3 + \mathcal{O}(r^5), \\ \dot{\theta} &= \omega(\mu) + b(\mu)r^2 + \mathcal{O}(r^4). \end{aligned} \tag{12}$$

Because we are interested in the dynamics near $\mu = 0$, it is natural to Taylor expand the coefficients in (12) about $\mu = 0$. Equation (12) becomes

$$\begin{aligned} \dot{r} &= \alpha'(0)\mu r + a(0)r^3 + \mathcal{O}(\mu^2 r, \mu r^3, r^5), \\ \dot{\theta} &= \omega(0) + \omega'(0)\mu + b(0)r^2 + \mathcal{O}(\mu^2, \mu r^2, r^4). \end{aligned} \tag{13}$$

where $'$ denotes differentiation with respect to μ and we have used the fact that $\alpha(0) = 0$.

2.2.5 The Poincaré–Andronov–Hopf Bifurcation theorem

Theorem 6. [The Poincaré–Andronov–Hopf Bifurcation Theorem] [3]
Consider the full normal form (13).
Then, for μ sufficiently small, *Case* 1, *Case* 2, *Case* 3, and *Case* 4 described below hold.

[3] we may refer to [26], P. 384

Case 1: $\alpha'(0) > 0$, $a(0) > 0$.
In this case the origin is an unstable fixed point for $\mu > 0$ and an asymptotically stable fixed point for $\mu < 0$, with an unstable periodic orbit for $\mu < 0$.
Case 2: $\alpha'(0) > 0$, $a(0) < 0$.
In this case the origin is an asymptotically stable fixed point for $\mu < 0$ and an unstable fixed point for $\mu > 0$, with an asymptotically stable periodic orbit for $\mu > 0$.
Case 3: $\alpha'(0) < 0$, $a(0) > 0$.
In this case the origin is an unstable fixed point for $\mu < 0$ and an asymptotically stable fixed point for $\mu > 0$, with an unstable periodic orbit for $\mu > 0$.
Case 4: $\alpha'(0) < 0$, $a(0) < 0$.
In this case the origin is an asymptotically stable fixed point for $\mu < 0$ and an unstable fixed point for $\mu > 0$, with an asymptotically stable periodic orbit for $\mu < 0$.

3 Synchronous Equations in Hindmarsh-Rose Networks

To derive synchronous equations in Hindmarsh-Rose Networks, we begin with the introduction of the Hindmarsh-Rose equation which governs the dynamics of single neuron. The equation has the following form.

$$\begin{cases} \dot{x} = f(x) + y - z + q, \\ \dot{y} = -y - 5x^2 + 1, \\ \dot{z} = \mu(b(x - x_0) - z), \end{cases} \tag{14}$$

where $f(x) = ax^2 - x^3$ and a, b, q, x_0 and μ are parameters. Moreover, μ is small parameter ($0 < \mu \ll 1$). We are now in a position to consider a network of excitatory HR neurons with bidirectional electrical coupling and unidirectional excitatory chemical coupling. The equations of motion are the following. For $i = 1, \ldots, n$,

$$\begin{aligned} \dot{x}_i &= f(x_i) + y_i - z_i + q + \sigma \sum_{j=1}^{n} g_{ij} x_j - g_s(x_i - v) \sum_{j=1}^{n} c_{ij} p(x_j), \\ \dot{y}_i &= -y_i - 5x_i^2 + 1, \\ \dot{z}_i &= \mu(b(x_i - x_0) - z_i), \end{aligned} \tag{15}$$

where

$\mathbf{G} =: (g_{ij})$, $\sum_{j=1}^{n} g_{ij} = 0$ for all i,

$\mathbf{C} =: (c_{ij})$, $c_{ij} = 0$ or 1, $c_{ii} = 0$, $\sum_{j=1}^{n} c_{ij} = k$ for all i,

$\mathbf{D} =: (d_{ij})$, and $d_{ij} = \begin{cases} -k \text{ if } i = j, \\ c_{ij} \text{ if } i \neq j, \end{cases}$

g_s is the strength of chemical coupling, v is the synaptic reversal potential, $p(x_j) =$

$\frac{1}{1+e^{-\lambda(x_j-\theta_s)}}$ is the chemically synaptic coupling function, k represents the number of chemical signals each neuron receives, and σ is the coupling strength for electrical synapses via gap junctions.
We next describe the synchronous equation of HR network (15). On the synchronous manifold $\{(x_1,y_1,z_1)=(x_2,y_2,z_2)=\cdots=(x_n,y_n,z_n)=(x,y,z)\}$, dynamics of HR network is governed by the following equations:

$$\begin{cases} \dot{x} = f(x) + y - z + q - kg_s(x-v)p(x) \\ \dot{y} = -y - 5x^2 + 1, \\ \dot{z} = \mu(b(x-x_0) - z), \end{cases} \tag{16}$$

where $f(x) = ax^2 - x^3$, $p(x) = \frac{1}{1+e^{-\lambda(x-\theta_s)}}$ and a, b, q, x_0, μ, v, λ and θ_s are parameters. Moreover, μ is small parameter $(0 < \mu \ll 1)$.
In [23], it was reported numerically that synchronous equation (16) generate some various mutisatable states as the parameter kg_s varies. Specifically, with the choice of the parameters $a = 2.6$, $b = 4$, $q = 4$, $x_0 = -1.6$, $v = 4$, $\lambda = 10$, $\theta_s = -0.25$ and the small parameter $\mu = 0.01$, they are able to observe the following mutistable states with various range of kg_s, which are summarized in Table 1.

Table 1: The dynamics of synchronous equation (16) with various range of kg_s. The multi-stability of (16) is observed with $kg_s \in [0.809, 0.85]$.

kg_s	$kg_s < 0.808$	$0.809 \le kg_s \le 0.813$	$0.814 \le kg_s \le 0.85$	$kg_s \ge 0.87$
Types	Stable regular bursting	Stable regular bursting Stable periodic solution	Stable regular bursting Stable steady state	Stable steady state

4 Dynamics of Synchronous Equations

In view of equation of (1), we first note that the corresponding fast and slow variables in (16) are, respectively, $\mathbf{x} = (x, y) \in \mathbb{R}^2$ and $\mathbf{y} = z \in \mathbb{R}$. Consequently, the fast limiting system of (16) has the following form

$$\begin{cases} \dot{x} = 2.6x^2 - x^3 + y - z + 4 - kg_s(x-2)\dfrac{1}{1+e^{-10(x+0.25)}}, \\ \dot{y} = -y - 5x^2 + 1, \end{cases} \tag{17a}$$

$$\dot{z} = 0, \tag{17b}$$

where z is regarded as a parameter. To apply geometric singular perturbation theory to equation (16), we shall construct a suitable critical manifold as well as the local and global geometric properties of the fast limiting system (17).

4.1 Critical manifolds

In this subsection, we shall choose critical manifolds with respect to equation (16). Let

$$N_{kg_s} = \{(x,y,z) \in \mathbb{R}^3 \mid 2.6x^2 - x^3 + y - z + 4 - kg_s(x-2)\frac{1}{1+e^{-10(x+0.25)}} = 0 \text{ and } -y - 5x^2 + 1 = 0\}.$$

For each fixed z, N_{kg_s} contains the set of the equilibriums of the fast subsystem Eq. (17a). The geometric singular perturbation theory needs to define a critical manifold from N_{kg_s} which satisfies Hypotheses 1, 2 and 5 of Eq. (16).
Let $(x,y,z) \in N_{kg_s}$ then

$$\begin{aligned} y &= 1 - 5x^2 \\ z &= 2.6x^2 - x^3 + (1 - 5x^2) + 4 - kg_s(x-2)\frac{1}{1+e^{-10(x+0.25)}} \\ &= -2.4x^2 - x^3 + 5 - kg_s(x-2)\frac{1}{1+e^{-10(x+0.25)}} \end{aligned}$$

Let $(x_0, y_0, z_0) \in N_{kg_s}$ and let $\tilde{x} = x - x_0$, $\tilde{y} = y - y_0$, $\tilde{z} = z - z_0$.

$$\begin{aligned} \dot{\tilde{x}} = \dot{x} &= 2.6x^2 - x^3 + y - z + 4 - kg_s(x-2)\frac{1}{1+e^{-10(x+0.25)}} \\ &= 2.6(\tilde{x}+x_0)^2 - (\tilde{x}+x_0)^3 + (\tilde{y}+y_0) - (\tilde{z}+z_0) + 4 - kg_s((\tilde{x}+x_0)-2)\frac{1}{1+e^{-10((\tilde{x}+x_0)+0.25)}} \\ &= 2.6(\tilde{x}^2 + 2x_0\tilde{x} + x_0^2) - (\tilde{x}^3 + 3x_0^2\tilde{x} + 3x_0\tilde{x}^2 + x_0^3) + (\tilde{y}+y_0) - (\tilde{z}+z_0) \\ &+ 4 - kg_s(\tilde{x}+x_0-2)\frac{1}{1+e^{-10((\tilde{x}+x_0)+0.25)}} \\ &= -\tilde{x}^3 + (2.6 - 3x_0)\tilde{x}^2 + (5.2x_0 - 3x_0^2)\tilde{x} + \tilde{y} - \tilde{z} + (2.6x_0^2 - x_0^3 + y_0 - z_0 + 4) \\ &- kg_s(\tilde{x}+x_0-2)\frac{1}{1+e^{-10((\tilde{x}+x_0)+0.25)}} \\ \dot{\tilde{y}} = \dot{y} &= -y - 5x^2 + 1 = -(\tilde{y}+y_0) - 5(\tilde{x}+x_0)^2 + 1 \\ &= -\tilde{y} - 5\tilde{x}^2 - 10x_0\tilde{x} + (-y_0 - 5x_0^2 + 1) = -\tilde{y} - 5\tilde{x}^2 - 10x_0\tilde{x} \\ \dot{\tilde{z}} = \dot{z} &= 0. \end{aligned}$$

To determine the stability and bifurcation points of a critical manifold which is a subset of N_{kg_s}, consider the linearized equation of above system

$$\begin{bmatrix} \dot{\tilde{x}} \\ \dot{\tilde{y}} \\ \dot{\tilde{z}} \end{bmatrix} = \begin{bmatrix} 5.2x_0 - 3x_0^2 - \frac{kg_s(1+e^{-10(x_0+0.25)}) + 10kg_s(x_0-2)e^{-10(x_0+0.25)}}{(1+e^{-10(x_0+0.25)})^2} & 1 & -1 \\ -10x_0 & -1 & 0 \\ 0 & 0 & 0 \end{bmatrix} \begin{bmatrix} \tilde{x} \\ \tilde{y} \\ \tilde{z} \end{bmatrix}$$

$$\det\begin{bmatrix} 5.2x_0 - 3x_0^2 - \frac{kg_s(1+e^{-10(x_0+0.25)})+10kg_s(x_0-2)e^{-10(x_0+0.25)}}{(1+e^{-10(x_0+0.25)})^2} - \lambda & 1 & -1 \\ -10x_0 & -1-\lambda & 0 \\ 0 & 0 & -\lambda \end{bmatrix}$$

$$= -\lambda \det\begin{bmatrix} 5.2x_0 - 3x_0^2 - \frac{kg_s(1+e^{-10(x_0+0.25)})+10kg_s(x_0-2)e^{-10(x_0+0.25)}}{(1+e^{-10(x_0+0.25)})^2} - \lambda & 1 \\ -10x_0 & -1-\lambda \end{bmatrix}$$

$$= -\lambda[\lambda^2 + (3x_0^2 - 5.2x_0 + \frac{kg_s(1+e^{-10(x_0+0.25)}) + 10kg_s(x_0-2)e^{-10(x_0+0.25)}}{(1+e^{-10(x_0+0.25)})^2} + 1)\lambda$$
$$+(3x_0^2 + 4.8x_0 + \frac{kg_s(1+e^{-10(x_0+0.25)}) + 10kg_s(x_0-2)e^{-10(x_0+0.25)}}{(1+e^{-10(x_0+0.25)})^2})]$$

Now, we consider the characteristic equation of the linearized equation that is important to determine the stability and bifurcation points of the corresponding critical manifold.
Let

$$D_{kg_s}(x_0,\lambda) = \lambda^2 + (3x_0^2 - 5.2x_0 + \frac{kg_s(1+e^{-10(x_0+0.25)}) + 10kg_s(x_0-2)e^{-10(x_0+0.25)}}{(1+e^{-10(x_0+0.25)})^2} + 1)\lambda$$
$$+(3x_0^2 + 4.8x_0 + \frac{kg_s(1+e^{-10(x_0+0.25)}) + 10kg_s(x_0-2)e^{-10(x_0+0.25)}}{(1+e^{-10(x_0+0.25)})^2}),$$

$$S_{kg_s}(x_0) = 3x_0^2 - 5.2x_0 + \frac{kg_s(1+e^{-10(x_0+0.25)}) + 10kg_s(x_0-2)e^{-10(x_0+0.25)}}{(1+e^{-10(x_0+0.25)})^2} + 1$$

and

$$P_{kg_s}(x_0) = 3x_0^2 + 4.8x_0 + \frac{kg_s(1+e^{-10(x_0+0.25)}) + 10kg_s(x_0-2)e^{-10(x_0+0.25)}}{(1+e^{-10(x_0+0.25)})^2}$$

then the sum of the roots of $D_{kg_s}(x_0,\lambda)$ is $-S_{kg_s}(x_0)$ and the product of the roots of $D_{kg_s}(x_0,\lambda)$ is $P_{kg_s}(x_0)$ for any $x_0 \in N_{kg_s}$.

From the Figure 2-5, we have

$$\begin{cases} R_{+-} \text{ for } x_5 < x_0 < x_6. \\ C_{++} \text{ for } x_3 < x_0 < x_4. \\ C_{--} \text{ for } x_7 < x_0 < x_3 \text{ or for } x_4 < x_0 < x_8. \\ R_{--} \text{ for } x_0 < x_5, \text{ for } x_6 < x_0 < x_7 \text{ or for } x_8 < x_0. \end{cases}$$

The number of characteristic roots with positive or negative real parts of $D_{kg_s}(x_0,\lambda) = 0$ with x_0 in different regions, where $R_{--}(R_{++})$ denotes two negative(positive) real roots, R_{+-} denotes one positive and one negative real roots, $C_{--}(C_{++})$ denotes two complex roots with negative(positive) real part.

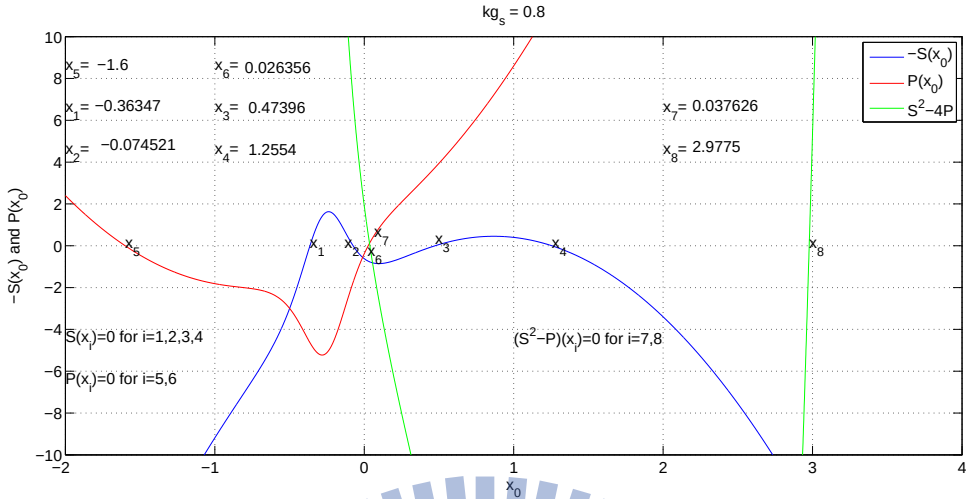

Figure 2: $-S_{kg_s}(x_0)$ and $P_{kg_s}(x_0)$ for $kg_s = 0.8$.

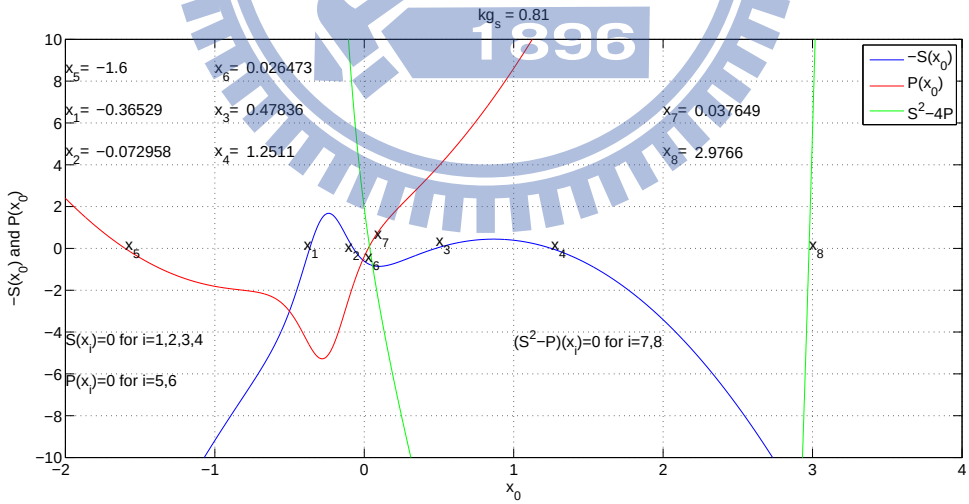

Figure 3: $-S_{kg_s}(x_0)$ and $P_{kg_s}(x_0)$ for $kg_s = 0.81$.

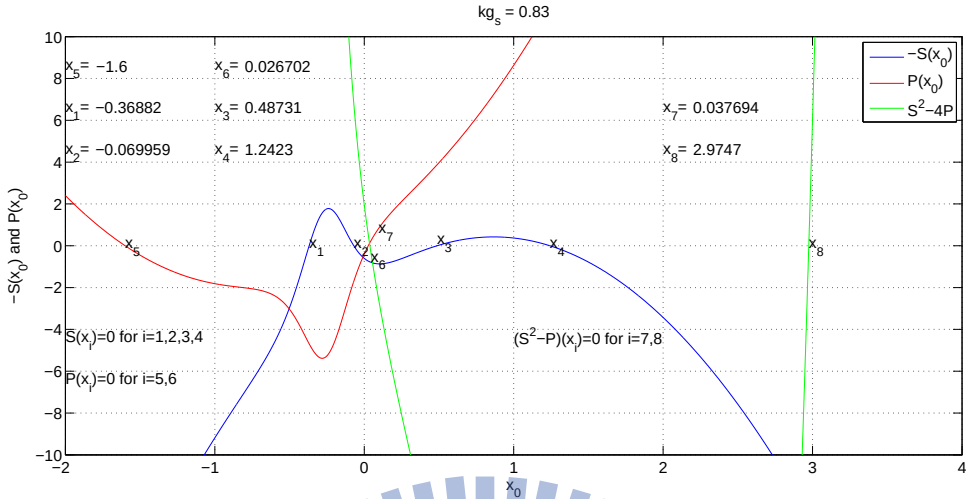

Figure 4: $-S_{kg_s}(x_0)$ and $P_{kg_s}(x_0)$ for $kg_s = 0.83$.

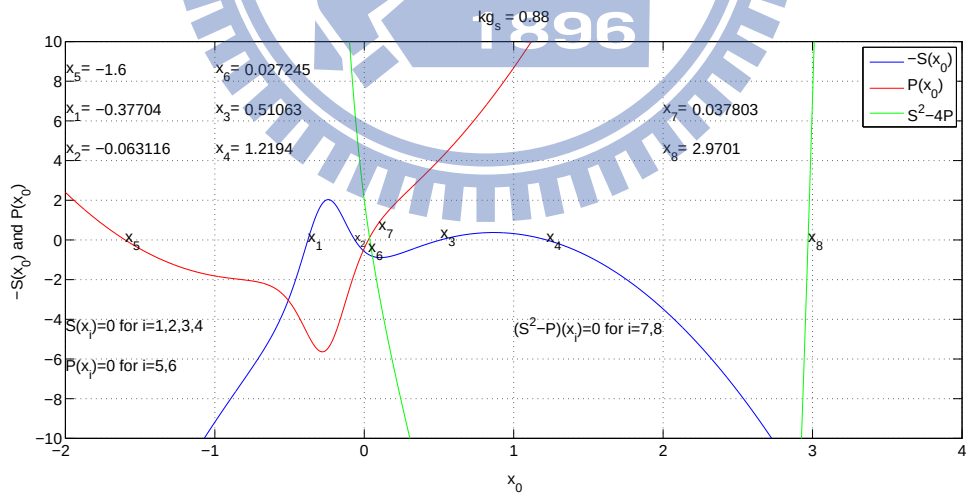

Figure 5: $-S_{kg_s}(x_0)$ and $P_{kg_s}(x_0)$ for $kg_s = 0.88$.

Let

$$M_0(kg_s;\delta) = \{\ (x,y,z) \in \mathbb{R}^3 \mid \\ 2.6x^2 - x^3 + y - z + 4 - kg_s(x-2)\frac{1}{1+e^{-10(x+0.25)}} = 0,\ -y - 5x^2 + 1 = 0, \\ x \in [-2, 2.5] \text{ but } x \notin \bigcup_{i=3}^{6} B(x_i;\delta)\ \}$$

be a critical manifold which satisfies the Hypotheses 1, 2 and 5 of Eq. (16) from N_{kg_s} for some $0 < \delta \ll 1$ then we can apply Geometric Singular Perturbation Theory to Eq. (16).

4.2 Dynamics on the fast subsystem (17a)

In this subsection, we consider the dynamics on the fast subsystem (17a) with fixed kg_s and treat z as the bifurcation parameter in $[-5, 8]$.

4.2.1 $kg_s = 0.8$

First, we consider $kg_s = 0.8$. When z varies, we discover twelve types of dynamical behaviors in numerical simulation. The tables (2 – 4) are the range of these types.

Table 2: The dynamics of the fast subsystem (17a) with various range of z. $x_4 \approx 1.2554 (z \approx -0.1653)$, $x_5 \approx -1.6 (z \approx 2.9520)$.

z	$-5 \le z < -0.1653$	$-0.1653 < z < 2.9520$	$2.9520 < z \le 3.2$	$3.3 \le z \le 3.4$
Types	Type I (see Figure (6(a)))	Type II (see Figure (6(b)))	Type III (see Figure (6(c)))	Type IV (see Figure (6(d))

Table 3: The dynamics of the fast subsystem (17a) with various range of z. $4.2 < z_{\text{HB1}} < 4.3$.

z	$3.5 \le z \le 4.1$	z_{HB1}	$4.3 \le z \le 4.8$	$4.9 \le z \le 5.2$
Types	Type V (see Figure (6(e))	Type VI (see Figure (6(f))	Type VII (see Figure (7(a))	Type VIII (see Figure (7(b))

Table 4: The dynamics of the fast subsystem (17a) with various range of z. $5.2 < z_{\mathrm{HB2}} < 5.3$, $x_3 \approx 0.47396 (z \approx 5.5744)$ and $x_6 \approx 0.026356 (z \approx 6.4836)$.

z	z_{HB2}	$5.3 \leq z < 5.5744$	$5.744 < z < 6.4836$	$6.4836 < z \leq 8$
Types	Type IX (see Figure (7(c))	Type X (see Figure (7(d))	Type XI (see Figure (7(e))	Type XII (see Figure (7(f))

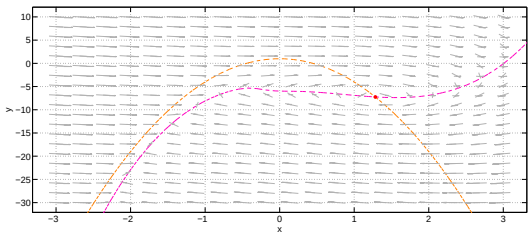

(a) Type I; $z = -0.5$ has only one stable fixed point

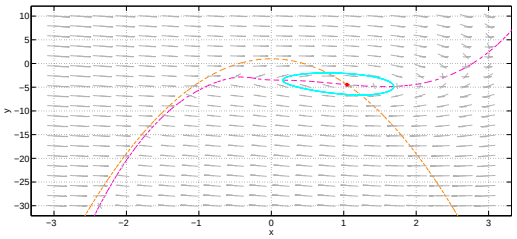

(b) Type II; $z = 2$ has only one unstable fixed point and only one stable periodic orbit

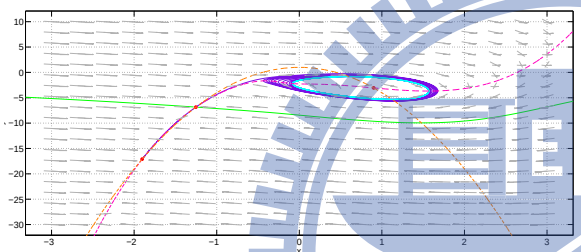

(c) Type III; $z = 3.2$ has three fixed point and only one stable periodic orbit

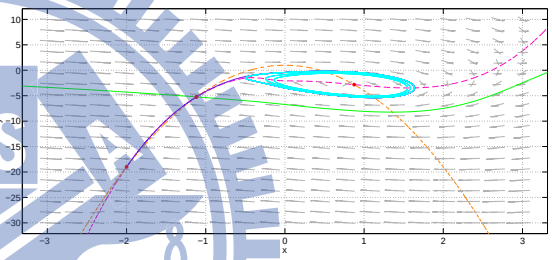

(d) Type IV; $z = 3.4$.

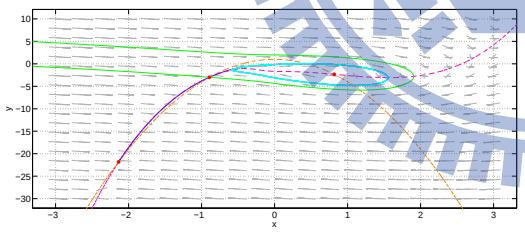

(e) Type V; $z = 3.8$

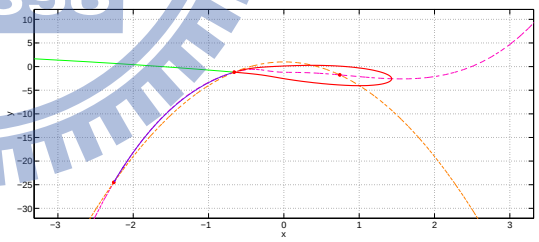

(f) Type VI; z_{HB1} is a parameter for Homoclinic Bifurcation, where $4.2 < z_{\mathrm{HB1}} < 4.3$.

Figure 6: For $kg_s = 0.8$, $x - y$ plane for z is a parameter.

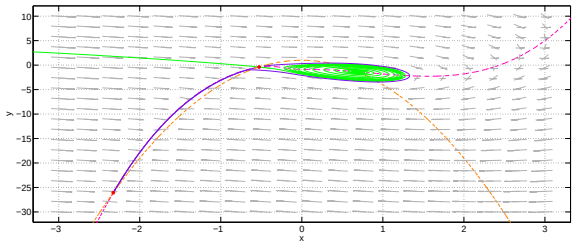

(a) Type VII; $z = 4.6$.

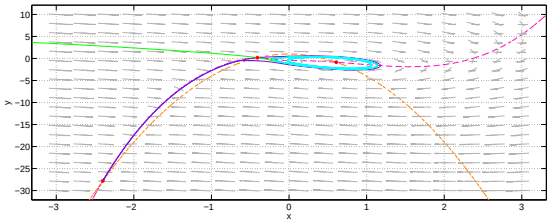

(b) Type VIII; $z = 5$ has two periodic orbits.

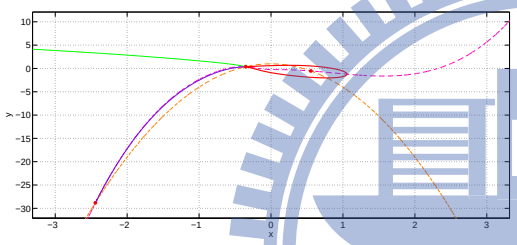

(c) Type IX; z_{HB2} is a parameter for Homoclinic Bifurcation, where $5.2 < z_{\mathrm{HB2}} < 5.3$.

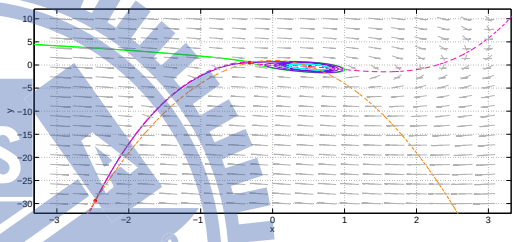

(d) Type X; $z = 5.4$.

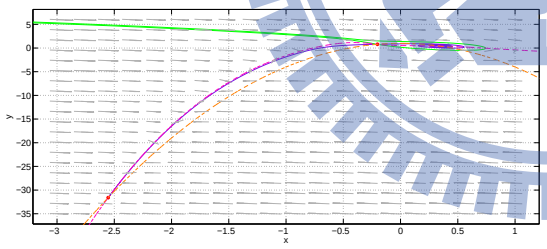

(e) Type XI; $z = 6$.

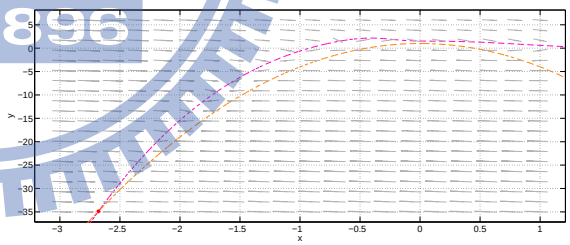

(f) Type XII; $z = 7$.

Figure 7: For $kg_s = 0.8$, $x - y$ plane for z is a parameter.

4.2.2 $kg_s = 0.81$

Second, we consider $kg_s = 0.81$. When z varies, we discover thirteen types of dynamical behaviors in numerical simulation. The tables (5 – 8) are the range of these types.

Table 5: The dynamics of the fast subsystem (17a) with various range of z. $x_4 \approx 1.2511 (z \approx -0.1081)$, $x_5 \approx -1.6 (z \approx 2.9520)$.

z	$-5 \leq z < -0.1081$	$-0.1081 < z < 2.9520$	$2.9520 < z \leq 3.31$	$3.32 \leq z \leq 3.46$
Types	Type I (see Figure (8(a)))	Type II (see Figure (8(b)))	Type III (see Figure (8(c)))	Type IV (see Figure (8(d))

Table 6: The dynamics of the fast subsystem (17a) with various range of z. $4.2 < z_{\mathrm{HB1}} < 4.3$.

z	$3.47 \leq z \leq 3.56$	$3.6 \leq z \leq 4.2$	z_{HB1}	$4.3 \leq z \leq 4.8$
Types	Type V (see Figure (8(e))	Type VI (see Figure (8(f))	Type VII (see Figure (9(a))	Type VIII (see Figure (9(b))

Table 7: The dynamics of the fast subsystem (17a) with various range of z. $x_3 \approx 0.47836 (z \approx 5.5730)$, $x_6 \approx 0.026473 (z \approx 6.5021)$ and $5.2 < z_{\mathrm{HB2}} < 5.3$.

z	$4.9 \leq z \leq 5.2$	z_{HB2}	$5.3 \leq z < 5.5730$	$5.5730 < z < 6.5021$
Types	Type IX (see Figure (9(c))	Type X (see Figure (9(d))	Type XI (see Figure (9(e))	Type XII (see Figure (9(f))

Table 8: The dynamics of the fast subsystem (17a) with various range of z.

z	$6.5021 < z \leq 8$
Types	Type XIII (see Figure (9(g))

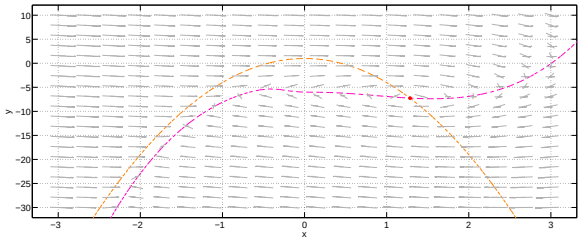

(a) Type I; $z = -0.5$ has only one stable fixed point

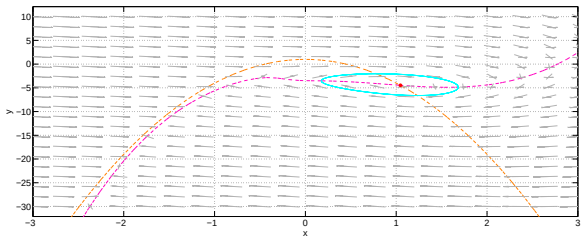

(b) Type II; $z = 2$ has only one unstable fixed point and only one stable periodic orbit

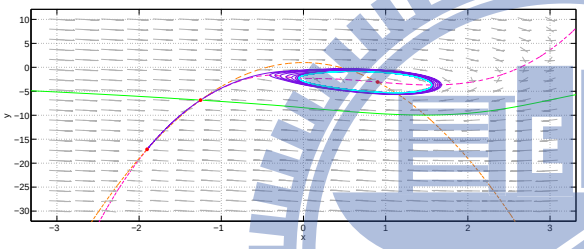

(c) Type III; $z = 3.2$ has three fixed point and only one stable periodic orbit

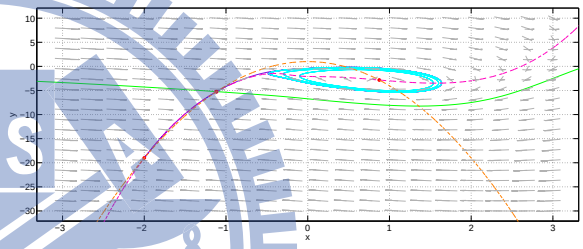

(d) Type IV;$z = 3.4$

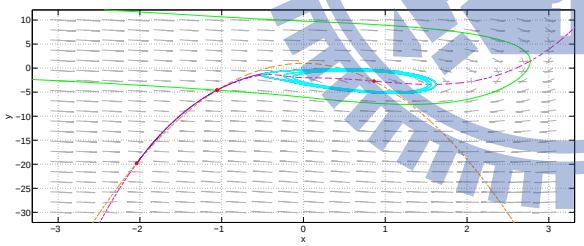

(e) Type V; $z = 3.5$

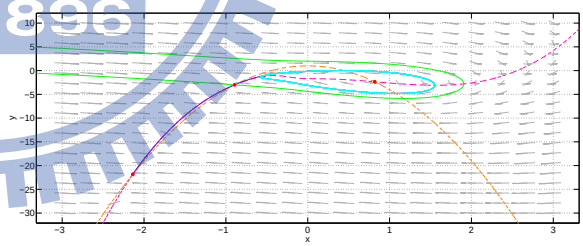

(f) Type VI; $z = 3.8$

Figure 8: For $kg_s = 0.81$, $x - y$ plane for z is a parameter.

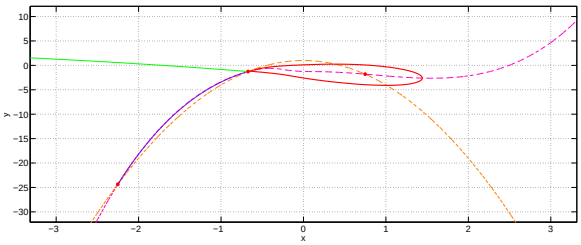

(a) Type VII; z_{HB1} is a parameter for Homoclinic Bifurcation, where $4.2 < z_{\mathrm{HB1}} < 4.3$

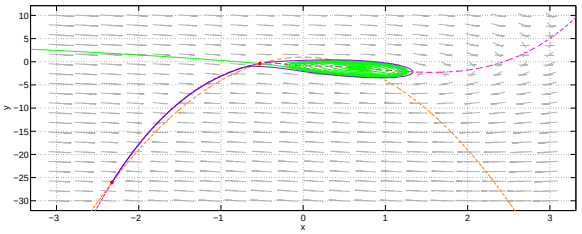

(b) Type VIII; $z = 4.6$

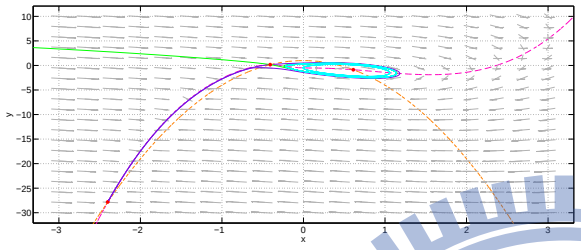

(c) Type IX; $z = 5$

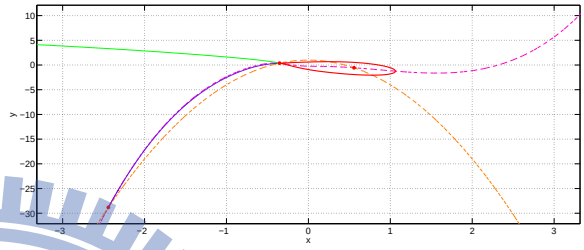

(d) Type X; z_{HB2} is a parameter for Homoclinic Bifurcation, where $5.2 < z_{\mathrm{HB2}} < 5.3$

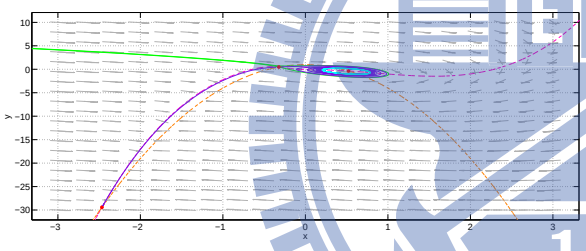

(e) Type XI; $z = 5.4$

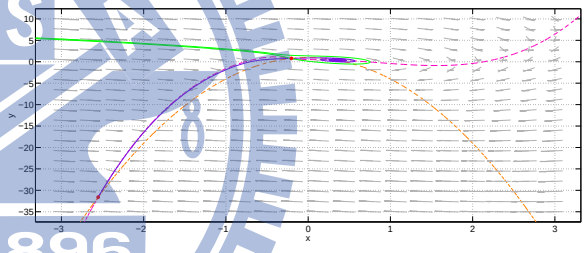

(f) Type XII; $z = 6$

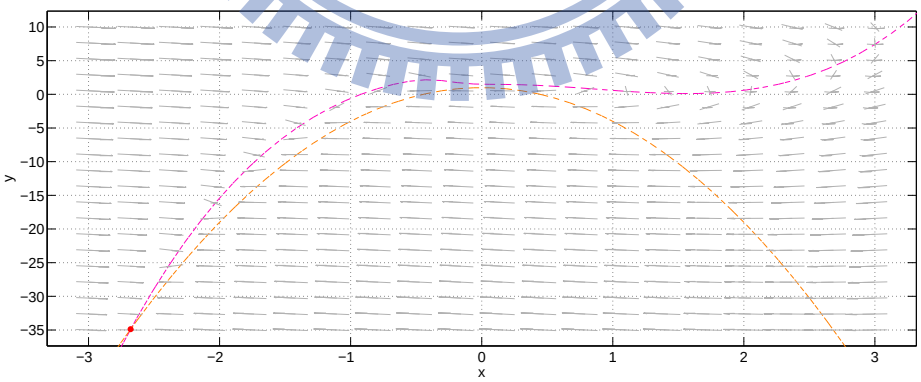

(g) Type XIII; $z = 7$

Figure 9: For $kg_s = 0.81$, $x - y$ plane for z is a parameter.

4.2.3 $kg_s = 0.83$

Third, we consider $kg_s = 0.83$. When z varies, we discover twelve types of dynamical behaviors in numerical simulation. The tables (9 – 11) are the range of these types.

Table 9: The dynamics of the fast subsystem (17a) with various range of z. $x_4 \approx 1.2423 (z \approx 0.0075)$, $x_5 \approx -1.6 (z \approx 2.9520)$.

z	$-5 \leq z < 0.0075$	$0.0075 < z < 2.9520$	$2.9520 < z \leq 3.4$	$3.5 \leq z \leq 3.8$
Types	Type I (see Figure (10(a)))	Type II (see Figure (10(b)))	Type III (see Figure (10(c)))	Type IV (see Figure (10(d))

Table 10: The dynamics of the fast subsystem (17a) with various range of z. $4.3 < z_{\mathrm{HB1}} < 4.4$.

z	$3.9 \leq z \leq 4.3$	z_{HB1}	$4.4 \leq z \leq 4.6$	$4.7 \leq z \leq 5.2$
Types	Type V (see Figure (10(e))	Type VI (see Figure (10(f))	Type VII (see Figure (11(a))	Type VIII (see Figure (11(b))

Table 11: The dynamics of the fast subsystem (17a) with various range of z. $5.2 < z_{\mathrm{HB2}} < 5.3$, $x_3 \approx 0.48731 (z \approx 5.5691)$ and $x_6 \approx 0.026702 (z \approx 6.5393)$.

z	z_{HB2}	$5.3 \leq z < 5.5691$	$5.5691 < z < 6.5393$	$6.5393 < z \leq 8$
Types	Type IX (see Figure (11(c))	Type X (see Figure (11(d))	Type XI (see Figure (11(e))	Type XII (see Figure (11(f))

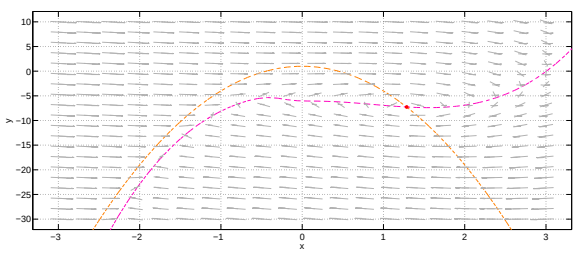

(a) Type I; $z = -0.5$ has only one stable fixed point

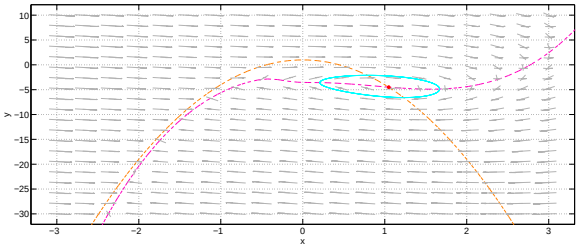

(b) Type II; $z = 2$ has only one unstable fixed point and only one stable periodic orbit

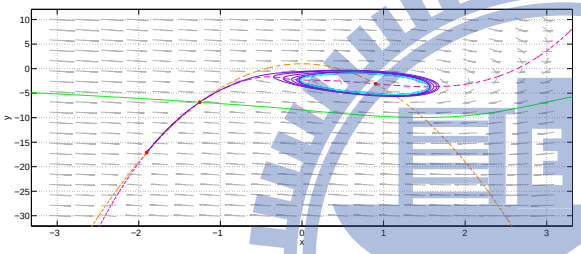

(c) Type III; $z = 3.2$ has three fixed point and only one stable periodic orbit

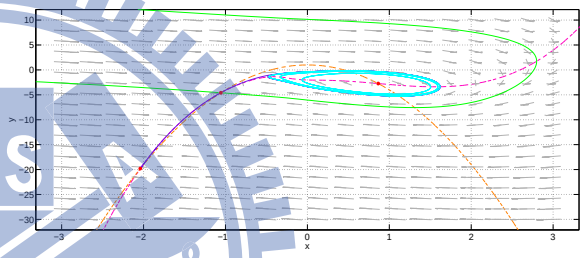

(d) Type IV; $z = 3.5$

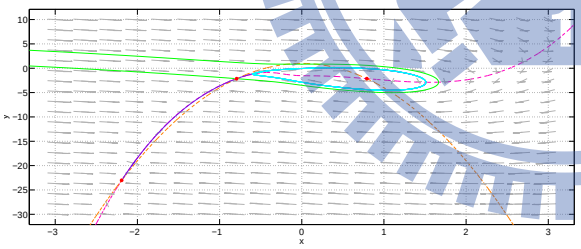

(e) Type V; $z = 4$

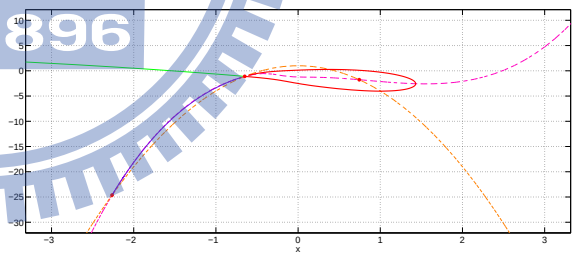

(f) Type VI; z_{HB1} is a parameter for Homoclinic Bifurcation, where $4.3 < z_{\mathrm{HB1}} < 4.4$

Figure 10: For $kg_s = 0.83$, $x - y$ plane for z is a parameter.

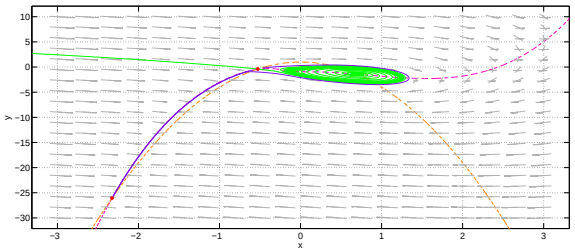

(a) Type VII; $z = 4.6$

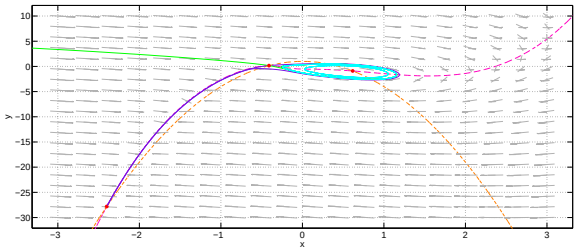

(b) Type VIII; $z = 5$

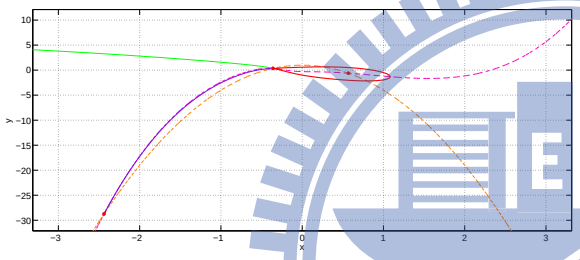

(c) Type IX; z_{HB2} is a parameter for Homoclinic Bifurcation, where $5.2 < z_{\mathrm{HB2}} < 5.3$

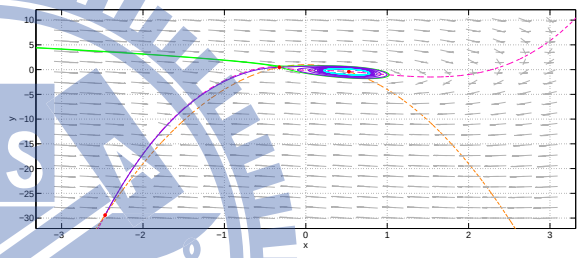

(d) Type X; $z = 5.4$

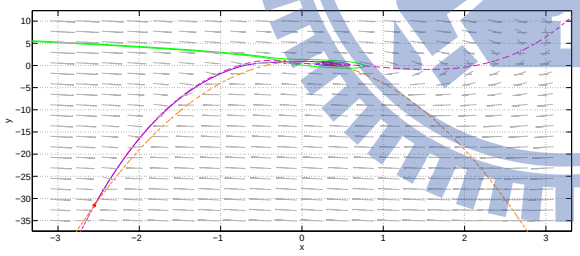

(e) Type XI; $z = 6$

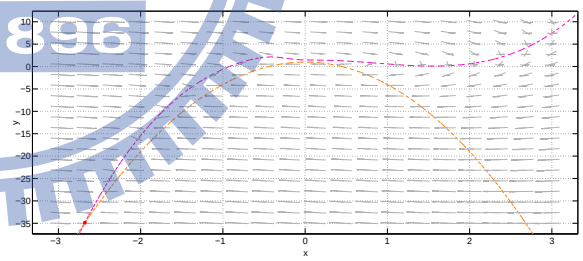

(f) Type XII; $z = 7$

Figure 11: For $kg_s = 0.83$, $x - y$ plane for z is a parameter.

4.2.4 $kg_s = 0.88$

Finally, we consider $kg_s = 0.8$. When z varies, we discover eleven types of dynamical behaviors in numerical simulation. The tables (12 – 14) are the range of these types.

Table 12: The dynamics of the fast subsystem (17a) with various range of z. $x_4 \approx 1.2194 (z \approx 0.3047)$, $x_5 \approx -1.6 (z \approx 2.9520)$.

z	$-5 \leq z < 0.3047$	$0.3047 < z < 2.9520$	$2.9520 < z \leq 3.5$	$3.6 \leq z \leq 3.7$
Types	Type I (see Figure (12(a)))	Type II (see Figure (12(b)))	Type III (see Figure (12(c)))	Type IV (see Figure (12(d))

Table 13: The dynamics of the fast subsystem (17a) with various range of z. $4.3 < z_{\mathrm{HB1}} < 4.4$, $5.1 < z_{\mathrm{HB2}} < 5.2$.

z	$3.8 \leq z \leq 4.3$	z_{HB1}	$4.4 \leq z \leq 5.1$	z_{HB2}
Types	Type V (see Figure (12(e))	Type VI (see Figure (12(f))	Type VII (see Figure (13(a))	Type VIII (see Figure (13(b))

Table 14: The dynamics of the fast subsystem (17a) with various range of z. $x_3 \approx 0.51063 (z \approx 5.5511)$ and $x_6 \approx 0.027245 (z \approx 6.6321)$.

z	$5.2 \leq z < 5.5511$	$5.5511 < z < 6.6321$	$6.6321 < z <\leq 8$
Types	Type IX (see Figure (13(c))	Type X (see Figure (13(d))	Type XI (see Figure (13(e))

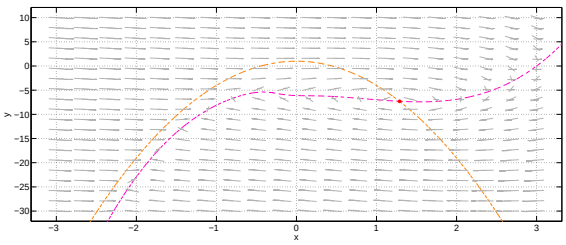

(a) Type I; $z = -0.5$ has only one stable fixed point

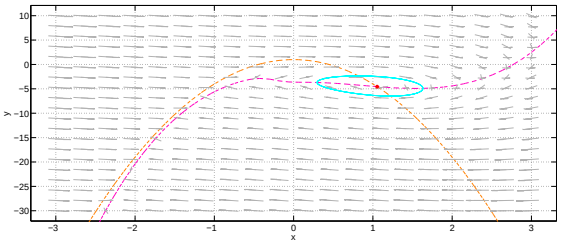

(b) Type II; $z = 2$ has only one unstable fixed point and only one stable periodic orbit

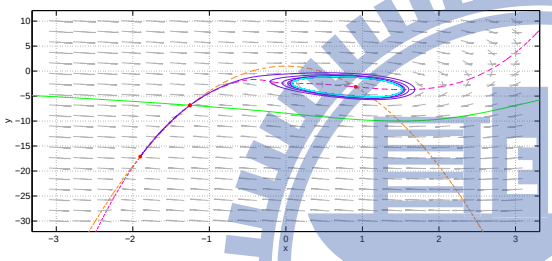

(c) Type III; $z = 3.2$ has three fixed point and only one stable periodic orbit

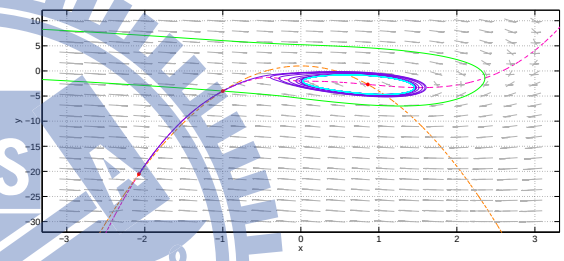

(d) Type IV; $z = 3.6$

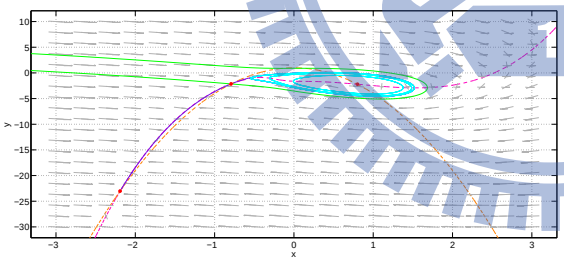

(e) Type V; $z = 4$

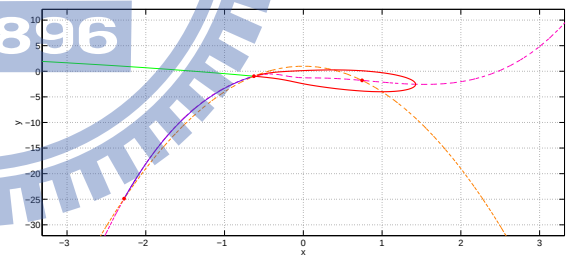

(f) Type VI; z_{HB1} is a parameter for Homoclinic Bifurcation, where $4.3 < z_{\mathrm{HB1}} < 4.4$

Figure 12: For $kg_s = 0.88$, $x - y$ plane for z is a parameter.

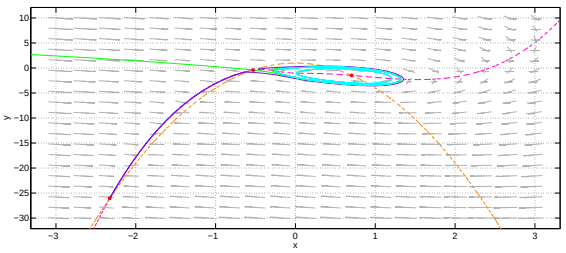

(a) Type VII; $z = 4.6$

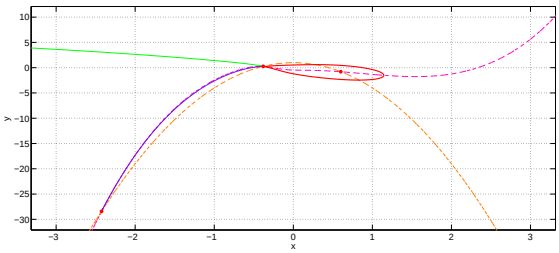

(b) Type VIII; z_{HB2} is a parameter for Homoclinic Bifurcation, where $5.1 < z_{\mathrm{HB2}} < 5.2$

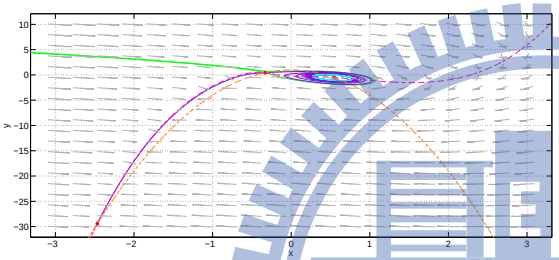

(c) Type IX; $z = 5.4$

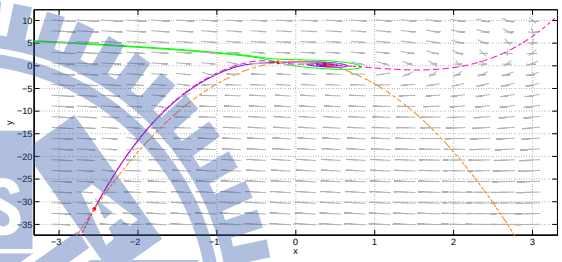

(d) Type X; $z = 6$

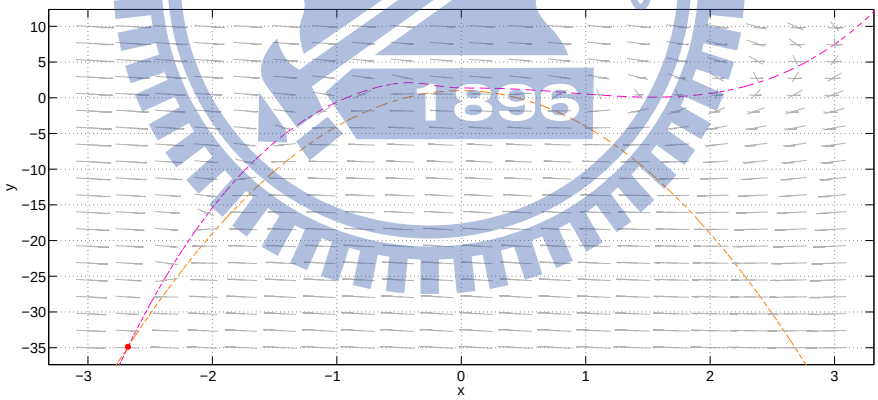

(e) Type XI; $z = 7$

Figure 13: For $kg_s = 0.88$, $x - y$ plane for z is a parameter.

4.3 Numerical results for various of kg_s

In this subsection, we show some pictures which associates with a solution orbit of Eq. (16).

(I) First we consider the case that $kg_s < 0.808$. From table (1), the attractor is unique regular bursting. In numerical simulation, we choose $kg_s = 0.8$ with two distinct initial values $\mathbf{x}_0^{(i)} = (x_0^{(i)}, y_0^{(i)}, z_0^{(i)})$, $i = 1, 2$ (See Figures 14 and 15), where $z_0^{(1)}$ in Type I (see Figure (6(a)) and $z_0^{(2)}$ in Type VII (see Figure (7(a)).

(II) Second we consider the case that $0.809 \leq kg_s \leq 0.813$. From table (1), the attractors have only two types regular bursting and periodic solution. In numerical simulation, we choose $kg_s = 0.81$ with two distinct initial values $\mathbf{x}_0^{(i)} = (x_0^{(i)}, y_0^{(i)}, z_0^{(i)})$, $i = 1, 2$ (See Figures 16 and 17), where $z_0^{(1)}$ in Type XI (see Figure (9(e)) and $z_0^{(2)}$ in Type I (see Figure (8(a)).

(III) Third we consider the case that $0.814 \leq kg_s \leq 0.85$. From table (1), the attractors have only two types regular bursting and steady state. In numerical simulation, we choose $kg_s = 0.83$ with three distinct initial values $\mathbf{x}_0^{(i)} = (x_0^{(i)}, y_0^{(i)}, z_0^{(i)})$, $i = 1, 2, 3$ (See Figures 18, 19 and 20), where $z_0^{(1)}$ in Type V (see Figure (10(e)), $z_0^{(2)}$ in Type I (see Figure (10(a)) and $z_0^{(3)}$ in Type XII (see Figure (11(f)).

(IV) Finally we consider the case that $kg_s \geq 0.87$. From table (1), the attractor is unique steady state. In numerical simulation, we choose $kg_s = 0.88$ with two distinct initial values $\mathbf{x}_0^{(i)} = (x_0^{(i)}, y_0^{(i)}, z_0^{(i)})$, $i = 1, 2$ (See Figures 21 and 22), where $z_0^{(1)}$ in Type VII (see Figure (13(a)) and $z_0^{(2)}$ in Type I (see Figure (12(a)).

Note:

1. for $kg_s = 0.8$, we have $x_3 \approx 0.47396$, $x_4 \approx 1.2554$, $x_5 \approx -1.6$, $x_6 \approx 0.026356$, $x_7 \approx 0.037626$ and the unstable fixed point is roughly $(0.020838, 0.99783, 6.4834)$.

2. for $kg_s = 0.81$, we have $x_3 \approx 0.47836$, $x_4 \approx 1.2511$, $x_5 \approx -1.6$, $x_6 \approx 0.026473$, $x_7 \approx 0.037649$ and the unstable fixed point is roughly $(0.02553, 0.99674, 6.5021)$.

3. for $kg_s = 0.83$, we have $x_3 \approx 0.48731$, $x_4 \approx 1.2423$, $x_5 \approx -1.6$, $x_6 \approx 0.026702$, $x_7 \approx 0.037694$ and the unstable fixed point is roughly $(0.034704, 0.99398, 6.5388)$.

4. for $kg_s = 0.88$, we have $x_3 \approx 0.51063$, $x_4 \approx 1.2194$, $x_5 \approx -1.6$, $x_6 \approx 0.027245$, $x_7 \approx 0.037803$ and the unstable fixed point is roughly $(0.056546, 0.98401, 6.6262)$.

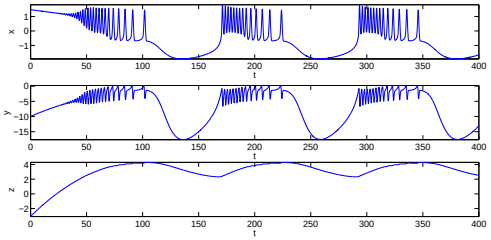

(a) Time Series

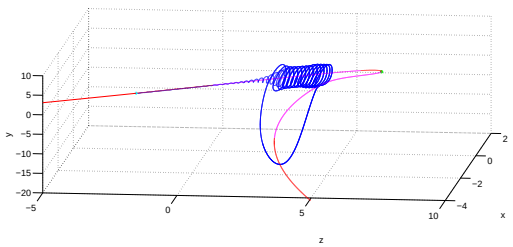

(b) Phase portrait

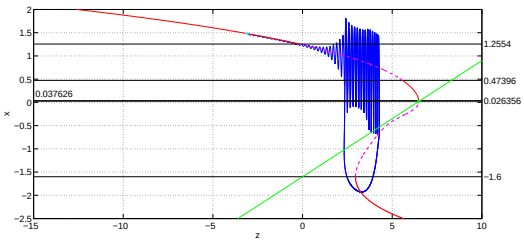

(c) Projection on $z-x$ plane

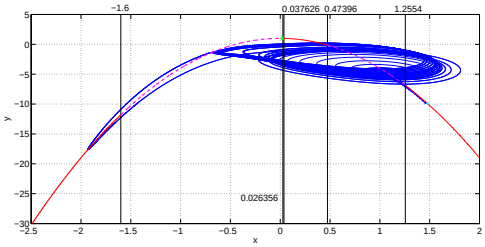

(d) Projection on $x-y$ plane

Figure 14: For $kg_s = 0.8$, a solution orbit of Eq. (16) with initial values $x_0^{(1)} = 1.48$, $y_0^{(1)} = -9.952$, $z_0^{(1)} = -3.0828$.

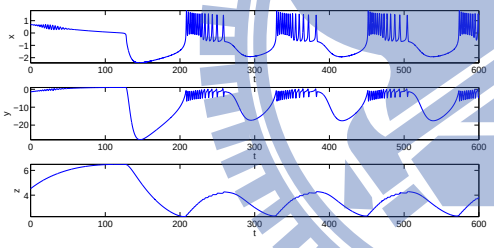

(a) Time Series

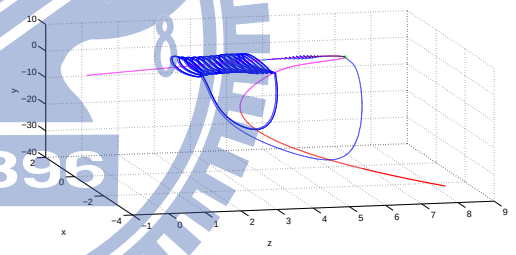

(b) Phase portrait

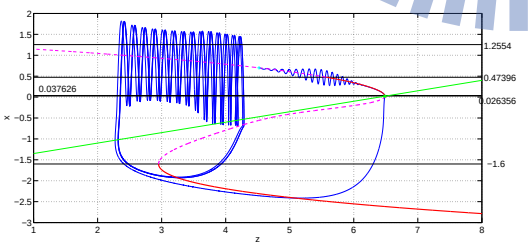

(c) Projection on $z-x$ plane

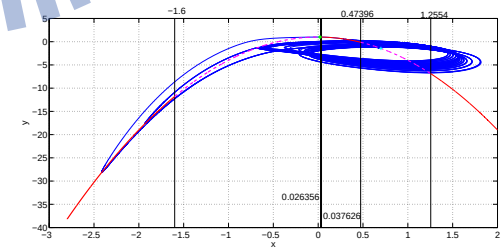

(d) Projection on $x-y$ plane

Figure 15: For $kg_s = 0.8$, a solution orbit of Eq. (16) with initial values $x_0^{(2)} = 0.7$, $y_0^{(2)} = -1.45$, $z_0^{(2)} = 4.5209$.

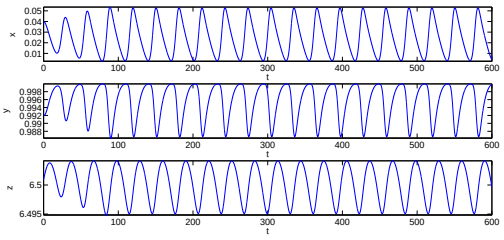

(a) Time Series

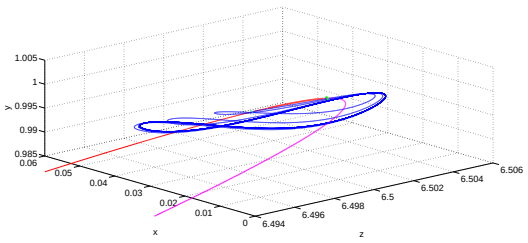

(b) Phase portrait

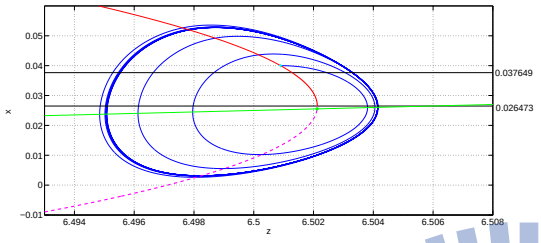

(c) Projection on $z - x$ plane

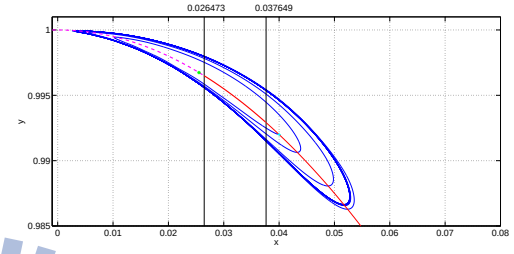

(d) Projection on $x - y$ plane

Figure 16: For $kg_s = 0.81$, a solution orbit of Eq. (16) with initial values $x_0^{(1)} = 0.04$, $y_0^{(1)} = 0.992$, $z_0^{(1)} = 6.5009$.

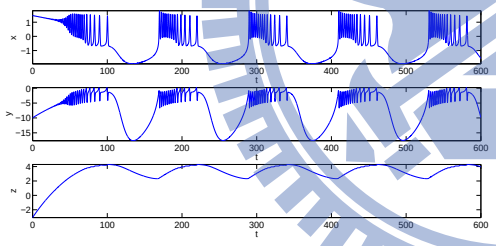

(a) Time Series

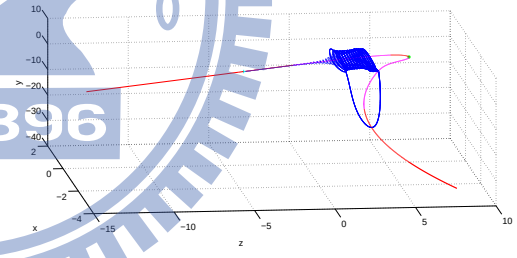

(b) Phase portrait

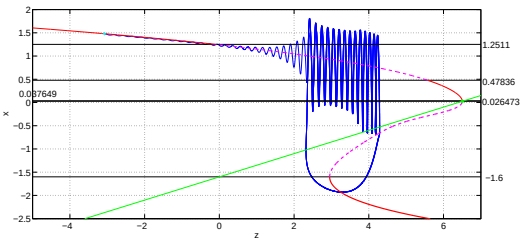

(c) Projection on $z - x$ plane

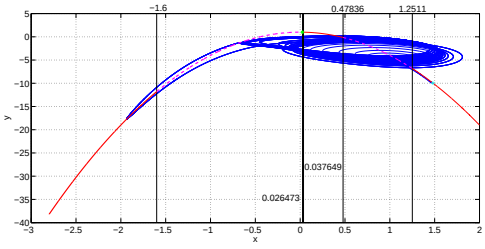

(d) Projection on $x - y$ plane

Figure 17: For $kg_s = 0.81$, a solution orbit of Eq. (16) with initial values $x_0^{(2)} = 1.48$, $y_0^{(2)} = -9.952$, $z_0^{(2)} = -3.0776$.

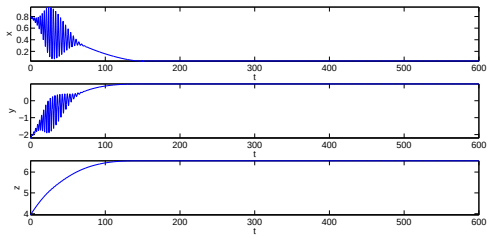

(a) Time Series

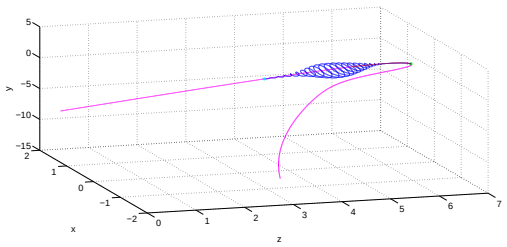

(b) Phase portrait

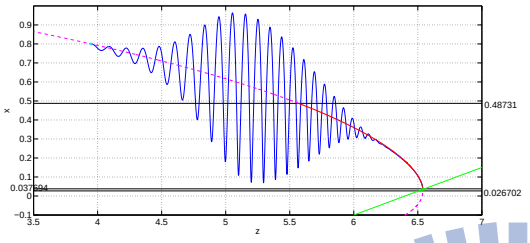

(c) Projection on $z-x$ plane

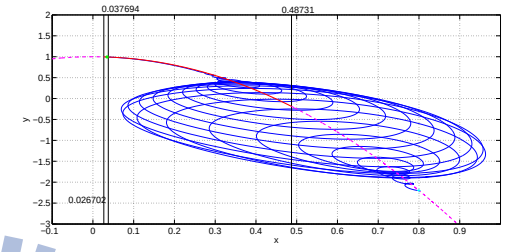

(d) Projection on $x-y$ plane

Figure 18: For $kg_s = 0.83$, a solution orbit of Eq. (16) with initial values $x_0^{(1)} = 0.8$, $y_0^{(1)} = -2.2$, $z_0^{(1)} = 3.948$.

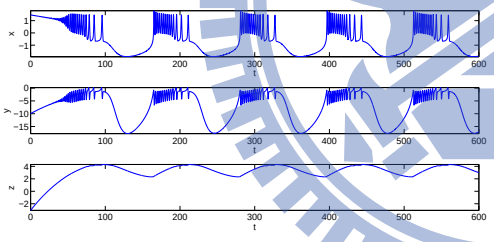

(a) Time Series

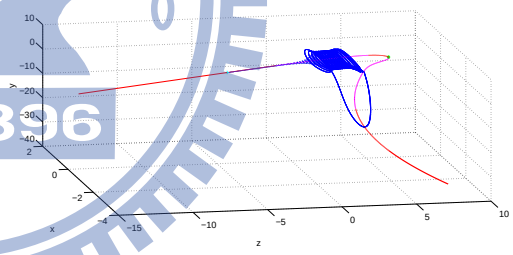

(b) Phase portrait

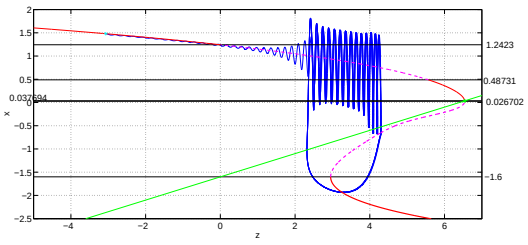

(c) Projection on $z-x$ plane

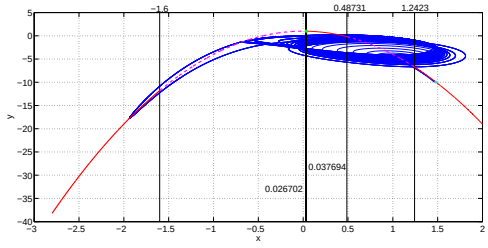

(d) Projection on $x-y$ plane

Figure 19: For $kg_s = 0.83$, a solution orbit of Eq. (16) with initial values $x_0^{(2)} = 1.48$, $y_0^{(2)} = -9.952$, $z_0^{(2)} = -3.0672$.

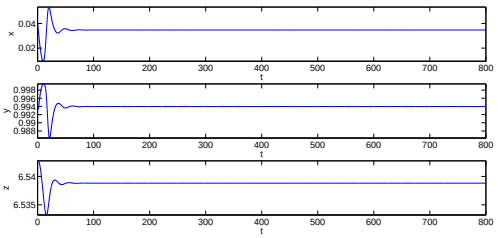

(a) Time Series

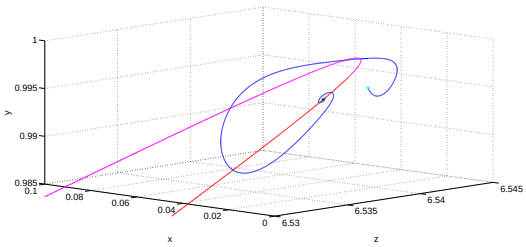

(b) Phase portrait

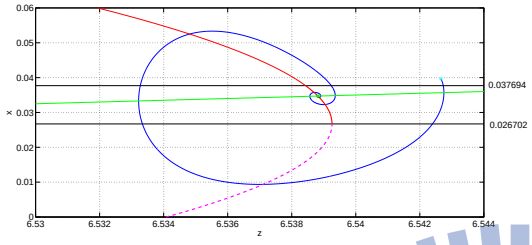

(c) Projection on $z - x$ plane

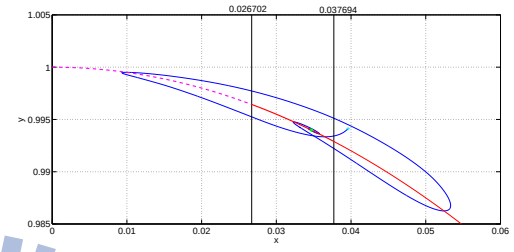

(d) Projection on $x - y$ plane

Figure 20: For $kg_s = 0.83$, a solution orbit of Eq. (16) with initial values $x_0^{(3)} = 0.039603$, $y_0^{(3)} = 0.99412$, $z_0^{(3)} = 6.5427$.

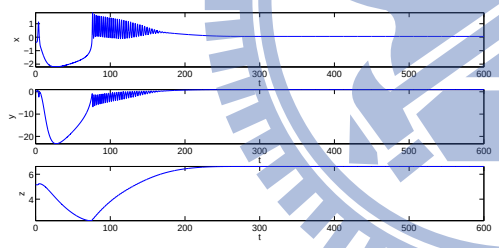

(a) Time Series

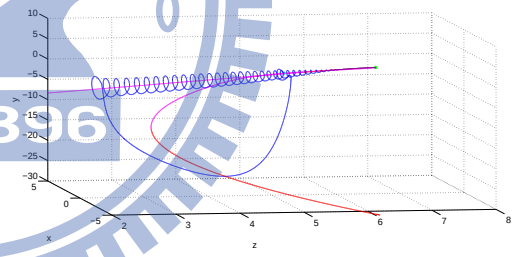

(b) Phase portrait

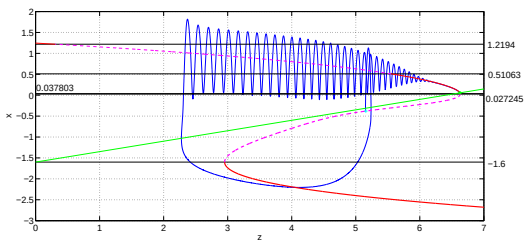

(c) Projection on $z - x$ plane

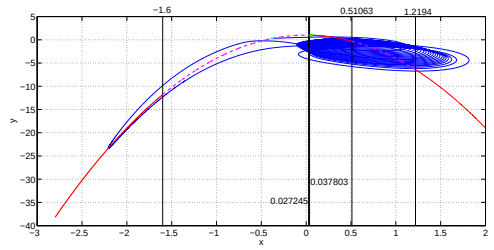

(d) Projection on $x - y$ plane

Figure 21: For $kg_s = 0.88$, a solution orbit of Eq. (16) with initial values $x_0^{(1)} = -0.38$, $y_0^{(1)} = 0.278$, $z_0^{(1)} = 5.1569$.

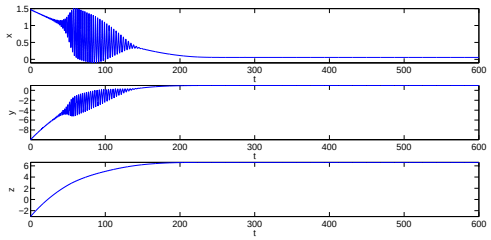

(a) Time Series

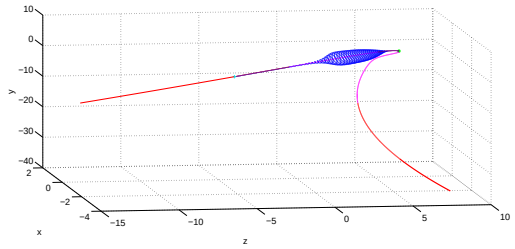

(b) Phase portrait

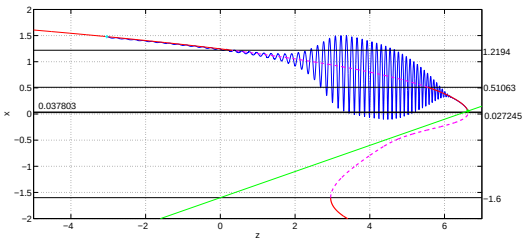

(c) Projection on $z - x$ plane

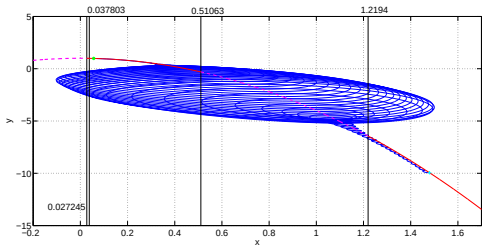

(d) Projection on $x - y$ plane

Figure 22: For $kg_s = 0.88$, a solution orbit of Eq. (16) with initial values $x_0^{(2)} = 1.48$, $y_0^{(2)} = -9.952$, $z_0^{(2)} = -3.0412$.

4.4 Analysis and conclusions

First, by The Poincaré–Andronov–Hopf Bifurcation Theorem, we have a Hopf bifurcation at $kg_s \approx 0.8131$ and there exists stable periodic solution to $kg_s < 0.8131$ (see Figure (23)).

Second, from subsection 4.1, we have

$$M_0(kg_s;\delta) = \{\ (x,y,z) \in \mathbb{R}^3 \mid 2.6x^2 - x^3 + y - z + 4 - kg_s(x-2)\frac{1}{1+e^{-10(x+0.25)}} = 0,\ -y - 5x^2 + 1 = 0,$$
$$x \in [-2, 2.5] \text{ but } x \notin \bigcup_{i=3}^{6} B(x_i;\delta)\ \}$$

is a critical manifold which satisfies the Hypotheses 1, 2 and 5 of Eq. (16) from N_{kg_s} for some chosen $0 < \delta \ll 1$ (e.g. $\delta = 0.0001$) then we can apply Fenichel's Second Theorem (theorem (3)) to Eq. (16). From subsection 4.2, we have the stable and unstable manifold of the equilibriums of the fast subsystem Eq. (36). So we know what are $W^s(M_0)$ and $W^u(M_0)$. Thus by Fenichel's Second Theorem (Theorem (3)), there exists manifolds $W^s(M_\varepsilon)$ and $W^u(M_\varepsilon)$ that are $O(\varepsilon)$ close and are diffeomorphic to $W^s(M_0)$ and $W^u(M_0)$ respectively, and they are each locally invariant under the flow of system (16), and C^r, including in ε, for any $r < \infty$. The large scale behaviors

that usually involve bursting can be explained (Figure 14, 15, 17, 18, 19, 21 and 22). This illustrates the power of using Singular perturbation theory to understand the global dynamical properties of realistic biological systems.

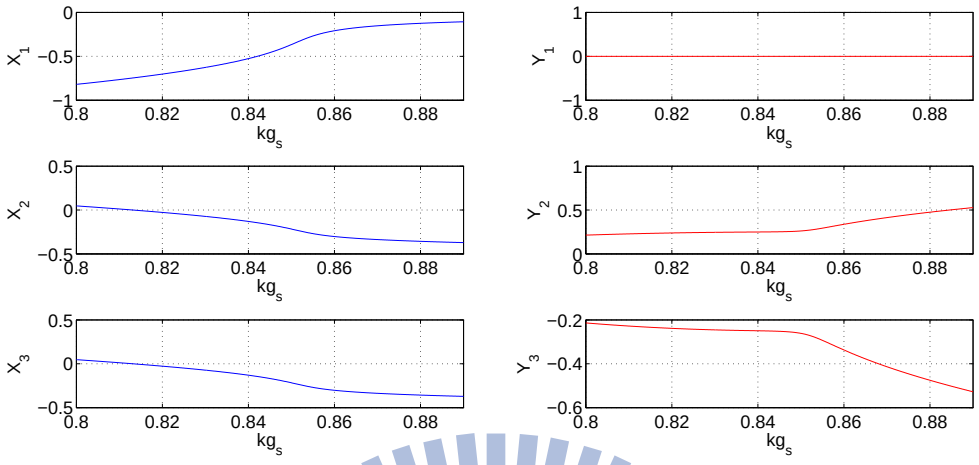

Figure 23: The eigenvalues ($\lambda_1 = x_1 + iy_1$, $\lambda_2 = x_2 + iy_2$ and $\lambda_3 = x_3 + iy_3$) of equilibrium of (16) to kg_s. $\mathrm{Re}\lambda_2 = 0$ and $\mathrm{Re}\lambda_3 = 0$ at $kg_s \approx 0.8131$.

References

[1] J.L. Hindmarsh and R.M. Rose, "A model of neuronal bursting using three coupled first order differential equations," Proc. Roy Soc. London Ser. B 221 (1984), 87-102.

[2] D. Terman, "Chaotic spikes arising from a model for bursting in excitable membranes," SIAM J. Appl. Math. 51 (1991), 1418-1450.

[3] D. Terman, "The transition from bursting to continuous spiking in an excitable membrane model," J. Nonlinear Sci. 2 (1992), 133-182.

[4] J. Rinzel and G.B. Ermentrout, "Analysis of neural excitability and oscillations Methods in Neuronal Modeling: From Ions to Networks," 2nd edn., C. Koch and I. Segev, eds, MIT Press, Cambridge, MA (1998), 251-291.

[5] G. Innocenti, A. Morelli, R. Genesio, and A. Torcini, "Dynamical phases of the Hindmarsh-Rose neuronal model: Studies of the transition from bursting to spiking chaos," Chaos, vol. 17, no. 4, p. 043128, 2007.

[6] E. M. Izhikevich, "Which model to use for cortical spiking neurons?," IEEE Trans. Neural Netw., vol. 15, no. 5, pp. 1063–1070, Sep. 2004.

[7] M. Storace, D. Linaro, and E. de Lange, "The Hindmarsh-Rose neuron model: Bifurcation analysis and piecewise-linear approximations," Chaos, vol. 18, no. 3, p. 033128, 2008.

[8] E. de Lange and M. Hasler, "Predicting single spikes and spike patterns with the Hindmarsh-Rose model," Biol. Cybern., vol. 99, no. 4, pp. 349–360, 2008.

[9] G. Innocenti and R. Genesio, "On the dynamics of chaotic spiking-bursting transition in the Hindmarsh-Rose neuron," Chaos, vol. 19, no. 2, p. 023124, 2009.

[10] D. Golomb and J. Rinzel, "Clustering in globally coupled inhibitory neurons," Phys. D 72 (1994), 259-282.

[11] D. Golomb, X.-J. Wang and J. Rinzel, "Synchronization properties of spindle oscillations in a thalamic reticular nucleus model," J. Neurophysiol. 72 (1994), 1109-1126.

[12] N. Kopell and G. LeMasson, "Rhythmogenesis, amplitude modulation and multiplexing in a cortical architecture," Proc. Nat. Acad. Sci. USA 91 (1994), 10586-10590.

[13] I. Belykh and M. Hasler, "Nonlinear dynamics: New directions," (Springer, 2013 (in press)) Chap. Patterns of synchrony in neuronal networks: the role of synaptic inputs.

[14] Jonq Juang and Yu-Hao Liang, "Cluster Synchronization in Networks of Neurons with Chemical Synapses," Chaos, vol. 24, no. 1, p. 013110, 2014.

[15] W. Singer, "Neuronal synchrony: A versatile code for the definition of relations?," Neuron , vol. 24, no. 1, pp. 49–65, Sep. 1999.

[16] P. J. Uhlhaas and W. Singer, "Neural synchrony in brain disorders: Relevance for cognitive dysfunctions and pathophysiology," Neuron, vol. 52, no. 1, pp. 155–168, Oct. 2006.

[17] S. Neuenschwander and W. Singer, "Long-range synchronization of oscillatory light responses in the cat retina and lateral geniculate nucleus," Nature, vol. 379, pp. 728–732, 1996.

[18] L. Glass, "Synchronization and rhythmic processes in physiology," Nature, vol. 410, no. 6825, pp. 277–284, 2001.

[19] C. M. Gray, P. Konig, A. K. Engel, and W. Singer, "Oscillatory responses in cat visual cortex exhibit inter-columnar synchronization which reflects global stimulus properties," Nature, vol. 338, pp. 334–337, 1989.

[20] R. Dzakpasu and M. Zochowski, "Discriminating differing types of synchrony in neural systems," Phys. D, vol. 208, no. 1–2, pp. 115–122,2005.

[21] G. Buzsaki, Rhythms of the Brain. New York: Oxford Univ. Press,2006.

[22] C. J. Stam, B. F. Jones, G. Nolte, M. Breakspear, and S. Ph, "Small-world networks and functional connectivity in alzheimer' s disease," Cereb. Cortex, vol. 17, no. 1, pp. 92–99, 2006.

[23] Jonq Juang, Yu-Hao Liang and Fang-Jhu Jhou, "Multistate and Multistage Synchronization of Hindmarsh-Rose Neurons With Excitatory Chemical and Electrical Synapses," Circuits and Systems I: Regular Papers, IEEE Transactions on (Volume:59 , Issue: 6), June 2012, 1335 - 1347

[24] Christopher K. R. T. Jones, Geometric singular perturbation theory. In: Johnson R (ed) Dynamical systems, Montecatibi Terme, Lecture Notes in Mathematics, vol 1609. Springer, Berlin, pp 44–118 (1995)

[25] Geertje Hek, "Geometric singular perturbation theory in biological practice," J. Math. Biol. (2010) 60:347–386, DOI 10.1007/s00285-009-0266-7

[26] Stephen Wiggins, Introduction to Applied Nonlinear Dynamical Systems and Chaos, Texts in applied mathematics, vol. 2, Springer, Second Edition, 2003

[27] Yuri A. Kuznetsov, Elements of Applied Bifurcation Theory, Applied Mathematical Sciences, vol. 112, Springer, Third Edition, 2004.

[28] Y. G. Zheng and Z. H. Wang "Time-delay effect on the bursting of the synchronized state of coupled Hindmarsh-Rose neurons," Chaos, vol. 22, no. 4, p. 043127, 2012.